R-7476

THE ROLE OF DISLOCATIONS IN THE STRESS-CORROSION CRACKING OF ALUMINUM ALLOYS

Final Report
(6 May 1967 through 5 May 1968)

June 1968

By

A. J. Jacobs

Prepared Under Contract N00019-67-C-0466

for

Naval Air Systems Command
Department of the Navy

By
Rocketdyne
A Division of North American Rockwell Corporation
Canoga Park, California

R-7476

THE ROLE OF DISLOCATIONS IN THE STRESS-CORROSION CRACKING OF ALUMINUM ALLOYS

Final Report
(6 May 1967 through 5 May 1968)

June 1968

By
A. J. Jacobs

Prepared Under Contract N00019-67-C-0466
for
Naval Air Systems Command
Department of the Navy

By
Rocketdyne
A Division of North American Rockwell Corporation
Canoga Park, California

FOREWORD

This report was prepared by the Chemical and Material Sciences organization of the Research Division of Rocketdyne, a division of North American Rockwell Corporation, in compliance with Contract No. N00019-67-C-0466, Naval Air Systems Command, U. S. Navy, covering the period from 6 May 1967 through 5 May 1968. The contract monitor was Mr. R. Schmidt.

The principal investigator was Dr. A. J. Jacobs with Dr. W. T. Chandler and Mr. E. D. Weisert providing technical supervision. The contributions of the following personnel are gratefully acknowledged: Professor G. Thomas of the University of California at Berkeley, D. O. Thompson, R. Chang, and H. W. Wiedersich of the North American Rockwell Science Center, with whom valuable discussions were held; B. S. Hickman and C. Heiple, also of the Science Center, who performed the X-ray and internal friction measurements, respectively; J. E. Hilzinger, who conducted the dislocation mobility measurements, and Miss A. Palyo, who prepared the thin films. B. S. Hickman was also a contributing author.

This document has been assigned Rocketdyne Report No. R-7476.

ABSTRACT

A thin-film examination of plastically deformed 7075-T6 and -T73 has shown that slip is confined to a smaller number of planes in the -T6 than in the -T73. X-ray line broadening measurements of ($MgZn_2$) particle size in a series of overaged 7075 conditions, together with stress-corrosion and tensile tests, have indicated that a correlation exists between particle size, time-to-failure, and yield strength. Each of these quantities undergoes a rapid change during the first 10 hours of aging at 350 F, and a much slower change thereafter. In cryogenic tensile tests, the yield strengths of -T6 and -T73 were shown to have a similar temperature dependence: the $T^{2/3}$ dependence, which is suggestive of a shearing mechanism, was obeyed from 20 to 160 K, and a smaller dependence was exhibited from 160 to 300 K. Dislocation mobility measurements have demonstrated a higher strain-rate sensitivity in -T6 than in -T73, and also a stronger tendency toward strain aging in the former temper. Amplitude-dependent internal friction studies have provided insight into dislocation-precipitate interactions, as well as into the early aging process in 7075.

CONTENTS

ILLUSTRATIONS

TABLES

INTRODUCTION

Considerable progress was made during the previous contract period toward understanding the mechanism of stress-corrosion cracking in 7075 and other high-strength aluminum alloys. A large body of evidence suggested that the basic difference between a susceptible temper such as 7075-T6 and a resistant temper such as -T73 resides in their respective capacities for plastic deformation at the tip of a crevice. The -T6 is limited in its ability to deform, primarily because of its high density of Guinier-Preston (G. P.) zones, while the -T73 can deform more easily because of its lower density of precipitate particles. A high stress concentration in -T6 is more likely to be relieved by mechanical fracture than plastic flow, whereas in -T73 plastic flow is a more likely mechanism. It was demonstrated that a rapid intergranular stress-corrosion failure could be induced in a -T73 specimen through the introduction of a notch. With its capacity for plastic flow thus limited, the -T73 behaves in a manner similar to -T6.

Because precipitate-dislocation interactions seemed so important in determining the stress-corrosion resistance of 7075, this year's effort was concentrated on: (1) a thorough characterization of the $MgZn_2$ particles (such parameters as size, inter-particle spacing, and particle density were measured using X-ray techniques); (2) a study of the deformation mechanisms in 7075-T6 and -T73, including thin-film microscopy and yield-strength measurements as a function of temperature; and (3) a study of precipitate-dislocation interactions by means of strain-rate sensitivity, stress relaxation, and internal friction measurements. The final part of the program dealt with a repetition of two experiments that were conducted during the previous contract period.

THIN-FILM STUDY OF PLASTICALLY DEFORMED 7075-T6 AND -T73

An experiment was described in the previous Final Report (Ref. 1), in which one series of 7075-T6 and another series of -T73 tensile specimens were deformed to various stress levels in the plastic range and then replicated to study the slip characteristics. Thin films have now been prepared from the same specimens. (The polishing and examination procedures are described in Ref. 2).

RESULTS AND DISCUSSION

A strong tendency toward restricted slip was observed in the -T6. This tendency is illustrated in Fig. 1, which shows dislocations arranged in discrete bands that are aligned in two mutually perpendicular [110]-type directions. In general, a much weaker trend toward restricted slip was found in -T73. A micrograph taken of a film that was electropolished from one side while the other side was masked is shown in Fig. 2. Appearing in this micrograph are two sharply outlined dislocation bands lying in (111) planes, according to stereographic analysis. The one-sided polishing technique was not necessary, but it seemed to help in revealing the banded structure.

The thin-film observations supported the results of the replica study, insofar as transgranular slip occurred in both tempers at all stress levels, and there was no evidence for preferential slip along grain boundaries.

Holl (Ref. 3) and Speidel (Ref. 4) have recently reported findings similar to those cited above. These investigators have suggested that the type of dislocation arrangement present after plastic deformation of aluminum determines whether the material is susceptible or resistant to stress corrosion. Holl observed that dislocations in highly susceptible material tended to remain on their original slip planes and slip was concentrated in well-defined bands. In material of low susceptibility, the dislocations formed uniformly distributed tangles, i.e., restricted slip

Figure 1. Dislocation Bands Indicative of Restricted Slip in 7075-T6

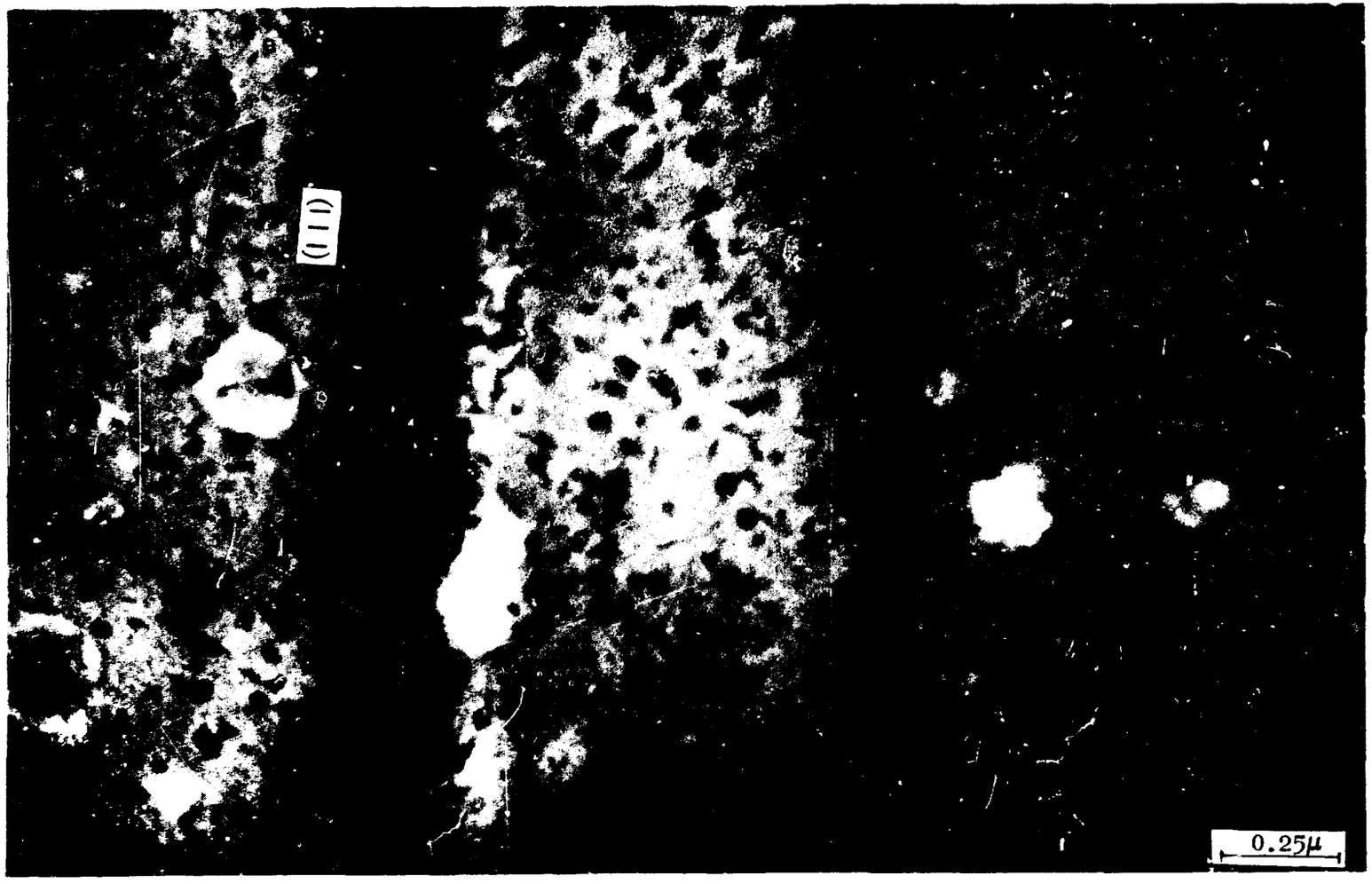

Figure 2. Dislocation Bands in 7075-T73

did not occur. Thus, according to Holl, dislocation pile-ups can exist in susceptible conditions, and by exerting a high stress concentration over a short length of grain boundary can transform a simple corrosion fissure into a propagating brittle crack. This process is repeated whenever the crack becomes arrested. Holl concludes that the overall distribution and nature of precipitates within the matrix, through their control over deformation behavior, are the important factors in determining stress-corrosion cracking susceptibility. The most susceptible condition is that containing G.P. zones or coherent precipitates; the most resistant condition contains noncoherent precipitates.

Speidel has reported observing in 7075-T6 long, straight narrow bands of high dislocation density extending across the grains; these bands were explained on the basis of precipitates being sheared during the deformation. In -T73, slip bands were reported to contain dislocations of irregular curvature and many dislocation loops; this structure was attributed to the bypassing of particles by moving dislocations. Speidel (Ref. 4) believes that the particular type of dislocation arrangement found in -T6 renders the structure susceptible to stress-corrosion cracking in one of several ways (Ref. 4). It should be noted that the shearing of G.P. zones or other particles has never been observed directly in 7075.

Ryum et al. (Ref. 5) have correlated the brittleness of some Al-Mg-Zn alloys with the dislocation structure present after deformation. In the most brittle alloys, dislocation movements took place in narrow bands through the grains and were not confined to precipitate-free zones as many investigators have proposed (e.g., Ref. 6). These bands were not only very narrow, but they were of low dislocation density. Bands were observed also in the more ductile alloys. These bands were wider and had a high dislocation density.

Thus, there is accumulating evidence that the restriction of slip to a small number of bands can be correlated, on the one hand, with susceptibility to stress-corrosion cracking (scc) and, on the other, with

limited ductility. Similar correlations have been found for homogeneous solid solutions wher the stacking fault energy is lowered by alloying elements (Ref. 7). What the critical factor is that disposes each alloy to scc remains a subject for speculation. The stress concentration at the head of a slip band, the average height of a slip step, and the limited ductility associated with the presence of slip bands are some of the main factors to be considered.

CHARACTERIZATION OF PRECIPITATE PARTICLES IN 7075 AND THE RELATIONSHIPS OF PRECIPITATE CHARACTERISTICS TO TENSILE AND STRESS-CORROSION PROPERTIES

It was shown in the previous contract period (Ref. 1) that a large number of stress-corrosion time-to-failure (t_f) data could be fitted to a straight line when plotted on a log scale against yield strength (4/3 of the applied stress). Theoretical (Ref. 8) and experimental studies (Ref. 9) of stress-rupture, fatigue, and other fracture phenomena have also disclosed a linear relationship between log t_f and the applied stress. The previous study also indicated that the particle density, and to a much lesser extent, the dislocation density, were important factors in determining t_f. Because 7075 is a precipitation hardening alloy and because its yield strength is presumably dependent on particle density and/or interparticle spacing, an effort has been made to correlate these quantities with each other and with stress-corrosion lifetime (t_f). This effort has consisted of four parts: (1) an X-ray analysis of particle characteristics, (2) a thin-film check of the X-ray results, (3) measurement of tensile properties, and (4) determination of stress-corrosion resistance. The samples for study covered a wide range of over-aged conditions.

HEAT TREATMENT

Material

The starting material for this study was a hand-forged 7075-T73 billet, measuring 4 by 6 by 8 inches and conforming to Military Specification A-22771-B. The composition reported by the supplier was as follows: 5.43-percent Zn, 2.41-percent Mg, 1.81-percent Cu, 0.25-percent Fe, 0.19-percent Cr, 0.07-percent Si, 0.04-percent Mn, 0.02-percent Ti, and the balance Al. Representative properties also reported by the supplier

were an electrical conductivity of 42.0-percent IACS and strength properties as follows:

Orientation	Yield Strength, psi	Tensile Strength, psi	Elongation, percent in 2 inches
Longitudinal	57,950	69,000	13.3
Long Transverse	56,000	67,450	7.1
Short Transverse	56,150	67,250	7.1

Experimental Procedure

Two 1-inch-thick longitudinal sections were cut from the as-received -T73 billet for re-solution heat treatment. This treatment consisted of a 2-1/3-hour hold at a furnace temperature of 895 F, followed by a water quench. A -T6 age was then conducted for 24-1/2 hours at a (furnace) temperature of 250 F.

Six short-transverse (S.T.) bars, each 7/8 by 1 by 4 inches, were cut from the first longitudinal section, and five S.T. bars, of the same dimensions as the first six, were cut from the second section. The 11 bars were over-aged at 350 F for times varying from 2 to 210 hours. These times are listed in Table 1.

TABLE 1

OVER-AGING TIMES AT 350 F FOR SPECIMENS USED IN CHARACTERIZATION STUDY

Specimen Number	Time at 350 F, hours
12	2
13	6
3	10
4	12
5	16
6	20
7	35
8	60
9	85
10	110
11	210

The various specimens for X-ray diffraction, thin-film examination, tensile and stress-corrosion tests were prepared from the 11 heat-treated bars. Descriptions of specimen geometry will be found in the appropriate sections.

X-RAY ANALYSIS

Experimental Procedure

In the following, the only precipitate considered is the $MgZn_2$ phase. X-ray reflections were observed from this phase during aging at the Bragg positions predicted from the published lattice parameters (Ref. 10). Some very weak reflections due to another phase (a copper phase?) were observed during the early stages of aging but these could not be identified. Their intensity was a factor of 10 lower than the $MgZn_2$ reflections and they have, therefore, been neglected. The main difficulty arose from the low intensity of the $MgZn_2$ reflections and the overlap of reflections that generally occurred. Anomalous intensity variations were also observed, which suggested considerable inhomogeneity between the samples.

Preliminary measurements indicated that the $20\bar{2}3$ CuK_α reflection from the $MgZn_2$, which occurs at a 2θ of 51.5 degrees, would be the most suitable reflection for line breadth analysis to obtain particle sizes. This reflection was not unduly affected by overlap of neighboring aluminum or $MgZn_2$ reflections, and had a reasonable intensity. Measurements were made using a G.E. diffractometer with a 1-degree beam slit and a 0.2-degree receiving slit on polished samples of the alloy aged for various times at 350 F. Slow step scanning of the reflection was done at 0.1-degree steps using 400 seconds counting time at each step. Pulse height discrimination was used to optimize the peak-to-background ratio. The data were collected on punch tape and then converted to cards for subsequent processing in the IBM 360 computer. To correct for instrumental broadening, data were collected in a similar fashion from the 220 CuK_α reflection of a standard quartz sample using 0.02-degree steps. The

computer program calculated and subtracted the background, corrected for Lorentz polarization, computed the Fourier coefficients of the broadened and control profiles and then computed the true Fourier coefficients of the reflection by deconvolution with the instrumental profile by the method of Stokes (Ref. 11).

In subsequent analysis of the data, it was assumed that the line broadening was due entirely to particle size effects. For reasons mentioned earlier, it was not possible to obtain the data from several orders of the same reflection, which is necessary to show the absence of strain broadening. However, experience with other systems (γ' precipitation in nickel aluminum alloys, omega phase in titanium alloys) has shown that strain broadening is not present during precipitation in these systems, and hence this should be a reasonable approximation. It should be noted that misfit strains between the aluminum matrix and the precipitate will not give rise to line broadening.

The mean column length ($\bar{M}$) perpendicular to the reflecting plane was then obtained from the data by plotting the cosine Fourier coefficients against L, as discussed by Warren (Ref. 12) and measuring the initial slope. The relation between $\bar{M}$ and the mean particle size depends on the particle size distribution function (Ref. 13), but within the limited accuracy of the current experiments it can be taken as being equivalent to the mean particle size.

Absolute volume fraction measurements were made on the sample annealed for 210 hours by measuring the relative intensities of the (220) aluminum and the (0004) $MgZn_2$ reflections. Because the precipitation occurs with (0001) $MgZn_2$ parallel to (110) aluminum, measurement of these parallel reflections should eliminate effects of preferred orientation that existed in the samples. The volume fraction of $MgZn_2$ phase was then calculated

from the relation:

$$\frac{V_1}{V_2} = \frac{I_1}{I_2} \frac{N_2^2}{N_1^2} \frac{|F_2|^2}{|F_1|^2} \frac{P_2}{P_1}$$

where

V_1 = volume fraction of aluminum

V_2 = volume fraction of $MgZn_2$

I_1 = intensity of 220 aluminum reflections

I_2 = intensity of 0004 $MgZn_2$ reflections

N_1 = unit cells of aluminum/unit volume = $1.51 \times 10^{-2}/\text{Å}^3$

N_2 = unit cells of $MgZn_2$/unit volume = $4.9 \times 10^{-3}/\text{Å}^3$

F_1 = scattering amplitude for aluminum = 15.7 (from International Tables for X-ray crystallography)

F_2 = mean scattering amplitude for $MgZn_2$ = 185

P_1 = multiplicity factor for (220) Al = 12

P_2 = multiplicity factor for (0004) $MgZn_2$ = 2

The scattering amplitude for $MgZn_2$ was obtained by using the Busing and Levy ORFLS computer program.

Results and Discussion

The results of the particle-size measurements are shown in Fig. 3. It can be seen that there is a rapid increase in particle size during the early stage of annealing with a suggestion of a slower increase at longer times. Some measurements were made during the later stages of aging using other reflections, in particular the 0004 and $21\bar{2}0$ reflections. Similar particle sizes were obtained from these reflections, as from the $20\bar{2}3$

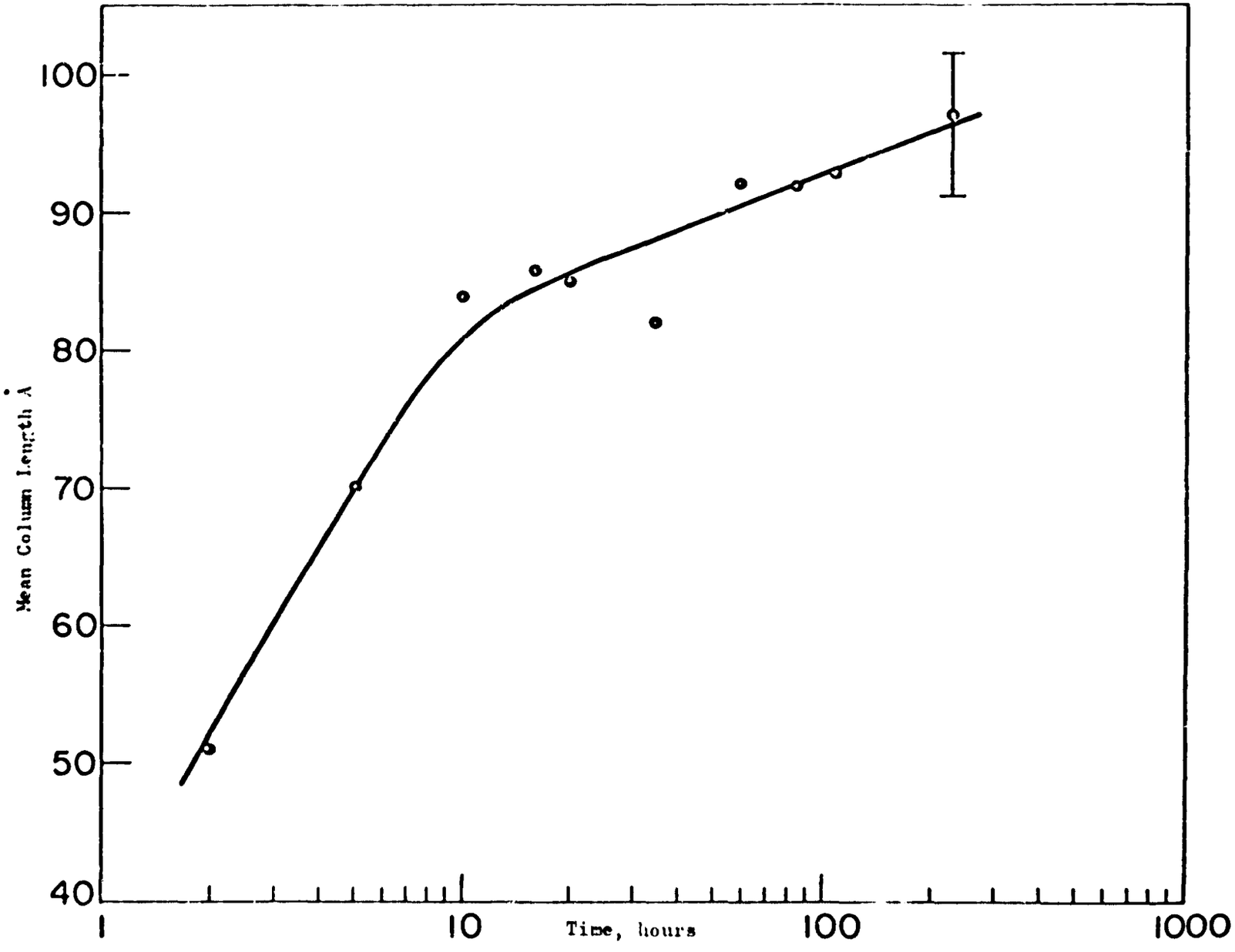

Figure 3. Mean Column Length of $MgZn_2$ Particles vs Over-Aging Time

which suggested that the particles were approximately equiaxed in shape. This is not in agreement with electron microscopy observations that show elongated particles (Ref. 6).

The volume-fraction measurements gave a value of 1.95 percent for the volume percentage of $MgZn_2$. Attempts to use this same method at shorter annealing times gave rather inconsistent results. This was possibly due to the difficulty in reliably measuring the 0004 intensity, but even allowing for this, there appeared to be real variations due to specimen inhomogeneity. It has been assumed in the above that the temperature factors for the two phases are similar (the reflections occur at not very different Bragg angles). The correctness of this assumption is perhaps questionable, but a considerable amount of work would have to be done to check its validity.

An approximate estimate of the volume fraction of the $MgZn_2$ during the earlier stages of annealing was obtained by measurement of the relative intensities of the $20\bar{2}3$ reflections, care being taken that the experimental conditions were kept constant. By combining these measurements with the above absolute measurement, the data shown in Fig. 4 were obtained. Although there is a wide scatter, these data suggest that precipitation of $MgZn_2$ is occurring during the first 20 hours or so of annealing, and after that the volume fraction remains relatively constant. The changes in particle size observed during the early stages of annealing would appear to be due to growth of precipitates by further precipitation rather than by particle coarsening.

Because the primary purpose of this phase of the program was to determine the interparticle spacing, this has been computed using the relation:

$$\text{Inter-particle Spacing} = \frac{\bar{M}}{\sqrt[3]{V_f}} - \bar{M}$$

where V_f = volume fraction of precipitate, and the results are shown in Table 2. It appears that the inter-particle spacing is essentially

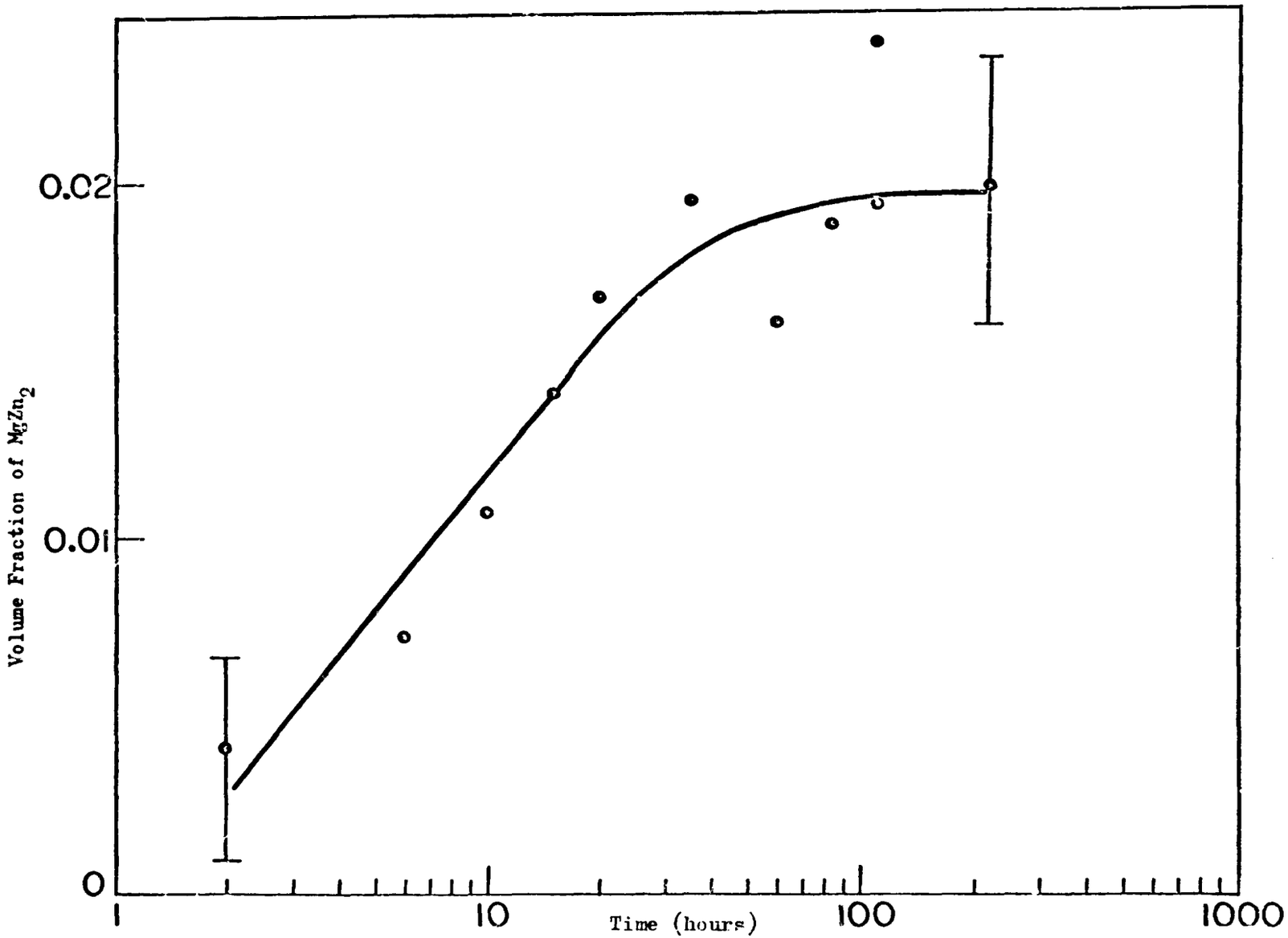

Figure 4. Volume Fraction of $MgZn_2$ vs Over-Aging Time

TABLE 2

SUMMARY OF X-RAY RESULTS

Over-aging Time, hours	$\bar{M}$, Å	V_f	$\sqrt[3]{V_f}$	Inter-particle Spacing, Å	$10^{15} \times N \left(\frac{\text{no.}}{\text{cm}^3}\right)$
2	51	0.004	0.16	270	30
6	70	0.007	0.19	300	20
10	84	0.011	0.22	300	19
16	86	0.014	0.24	280	22
20	85	0.017	0.26	250	28
35	82	0.0195	0.27	225	35
60	92	0.016	0.25	280	21
85	92	0.019	0.27	250	24
110	94	0.022	0.28	240	26
210	97	0.0195	0.27	265	21

constant. This is perhaps not unexpected if significant particle coarsening does not occur, since the inter-particle spacing will be determined by the initial scale of nucleation.

THIN-FILM EXAMINATION

A thin film for electron microscope examination was prepared from the most highly over-aged condition (No. 11, 210 hours at 350 F) used in the X-ray study. The object was to conduct a rapid, preliminary check of the X-ray results.

Procedure

The thin film had the same orientation in the forging as the X-ray diffraction specimen. The polishing procedure is detailed in an earlier publication (Ref. 2). Examination was carried out in an Hitachi HU-11 microscope operated at 100 kv.

Results and Discussion

Micrographs of two different areas are shown in Fig. 5 and 6. A previously obtained micrograph of a specimen that was aged for 10 hours at 350 F is shown for comparison in Fig. 7.

A complex array of precipitate morphologies is immediately apparent in the micrographs. The high degree of heterogeneity is also apparent from a comparison of the two areas in the same specimen (Fig. 5 and 6).

The major precipitate species (assumed to be $MgZn_2$ on the basis of electron diffraction evidence Ref. 2) seems to have grown by more than the ~15 percent indicated by the X-ray results (Table 2), as the over-aging time was increased from 10 to 210 hours. More importantly, the volume fraction of $MgZn_2$ seems to have decreased, and the inter-particle spacing to have increased, which is contrary to the X-ray findings.

Figure 5. Micrograph of 7075-T6 Specimen After Over-Aging for 210 Hours at 350 F

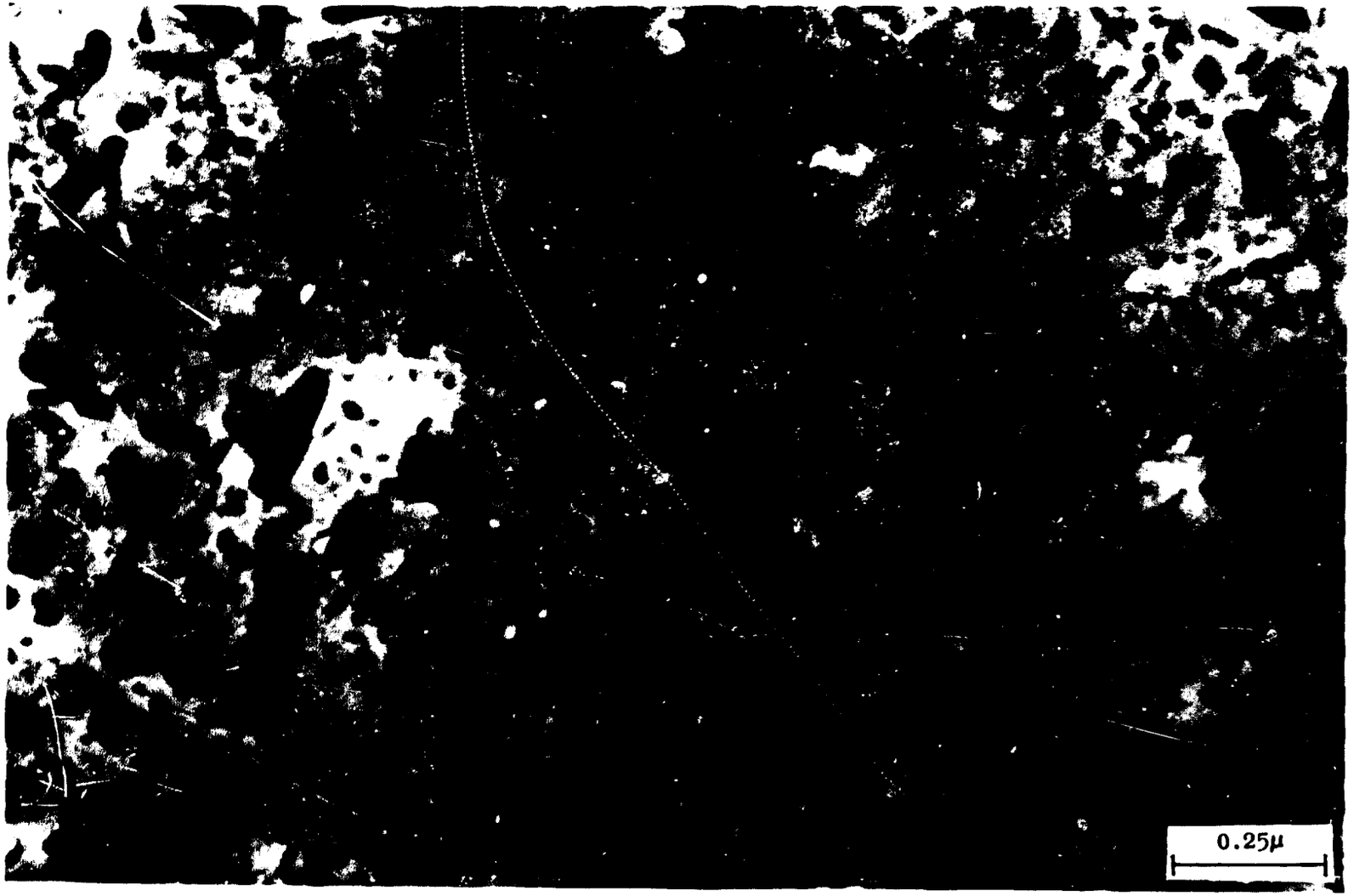

Figure 6. Micrograph of Another Area in the Same Specimen Shown in Fig. 5

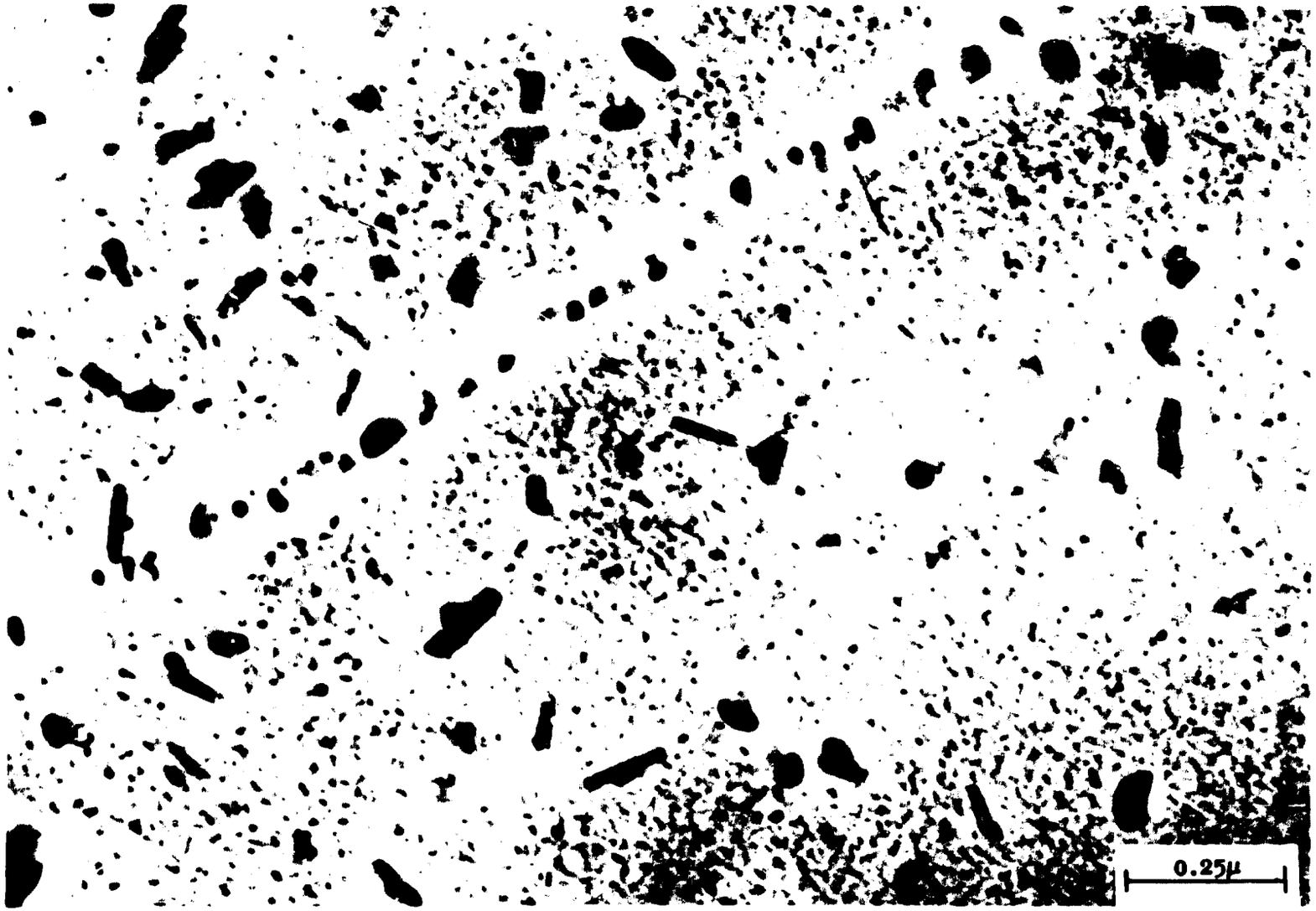

Figure 7. Micrograph of 7075-T6 Specimen After Over-Aging for 10 Hours at 350 F

Further interpretation of the micrographs will not be attempted at this time. Quantitative metallography, carried out on thin films of 7075-T6, -T73, and other over-aged conditions, is urgently required to establish the yield-strength dependence on interparticle spacing, or the independence suggested by the X-ray work.

TENSILE TESTS

Experimental Procedure

Tensile tests were conducted in duplicate on 1/8-inch rounds, the same type of specimen used in the stress-corrosion tests (Fig. 10). A 60,000-pound-capacity Riehle tensile testing machine was employed.

Results

The test results are summarized in Table 3. A plot of the tensile properties versus (log) aging time is shown in Fig. 8. The decrease in yield strength (Y.S.), unlike that in tensile strength (T.S.), is observed to take place in two steps. In the first step, between 2 and 10 hours, the Y.S. undergoes a 27-percent decrease; during the next 200 hours, this property drops only an additional 37 percent. The T.S. decreases uniformly over the entire over-aging range. The ductility, as measured by percent elongation in 1/2-inch, rises at an increasing rate up to t = 16 hours, whereupon it levels out at ~12 percent.

STRESS-CORROSION TESTS

If conventional stress-corrosion specimens were used in this phase of the program, most of the heat-treated conditions to be studied would take probibitively long times to fail in a 3-1/2-percent NaCl solution. It was demonstrated during the last contract period (Ref. 1) that a rapid, intergranular stress-corrosion failure could be induced in a -T73 specimen through the introduction of a notch. Thus, to achieve rapid failures in a broad

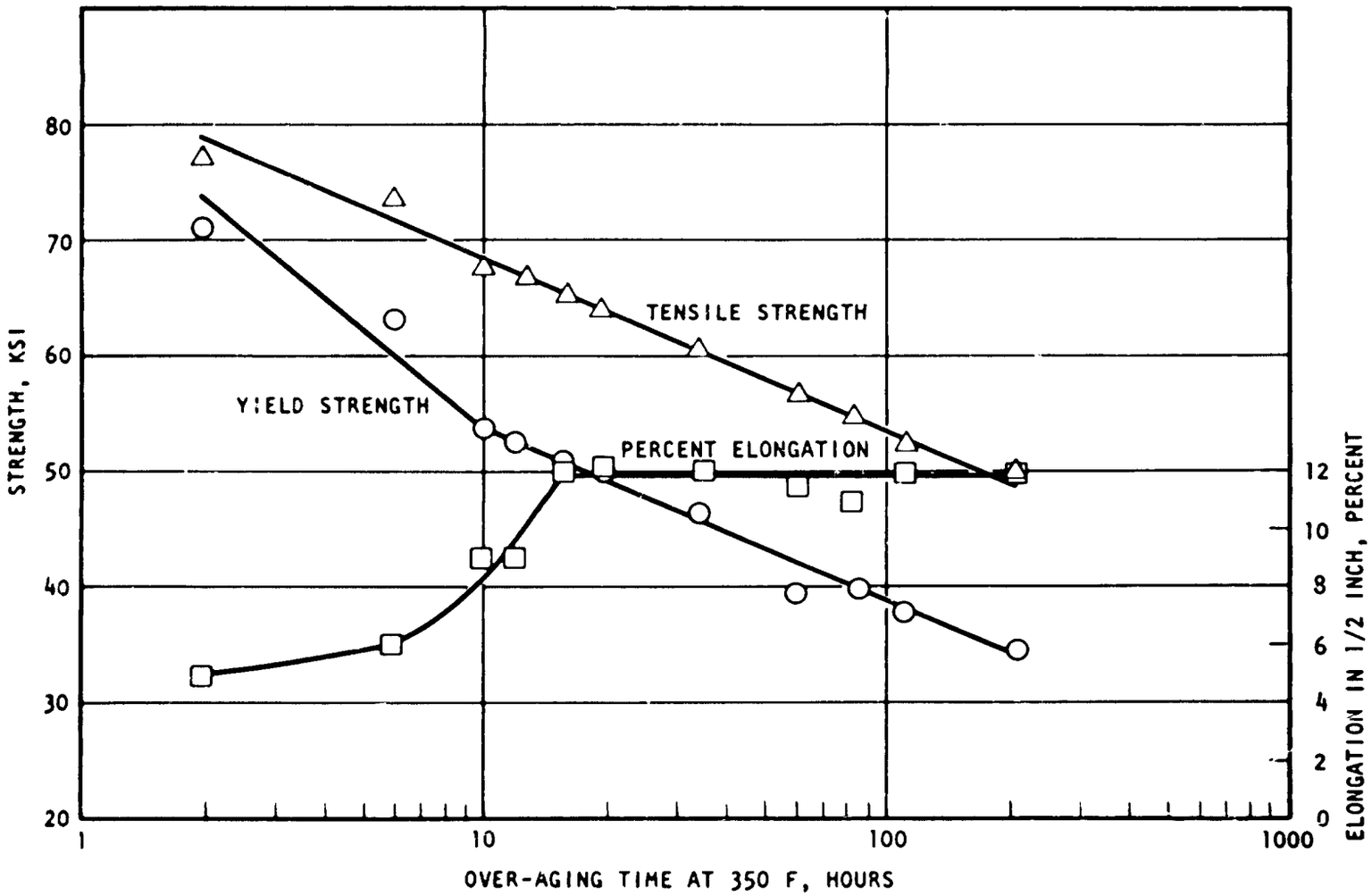

Figure 8. Tensile Properties of Over-Aged 7075 Plotted as a Function of Aging Time

TABLE 3

TEST RESULTS

Specimen Number	Over-Aging Time, hours	Y.S., ksi	Average Y.S., ksi	T.S., ksi	Average T.S., ksi	Elongation in 1/2-Inch, percent	Average Elongation, percent
121	2	72.0	70.9	76.0	77.0	4.0	5.0
122	2	69.7		78.0		6.0	
131	6	63.0	62.9	73.2	73.6	6.0	6.0
132	6	62.8		74.0		6.0	
31	10	53.7	53.8	67.5	67.5	10.0	9.0
32	10	53.8		67.5		8.0	
41	12	52.8	52.5	68.0	67.0	9.0	9.0
42	12	52.2		65.9		9.0	
51	16	50.2	50.7	64.0	65.2	12.0	12.0
52	16	51.2		66.3		12.0	
61	20	48.9	49.7	63.4	64.1	12.0	12.0
62	20	50.4		64.7		12.0	
71	35	45.9	46.1	60.9	60.8	12.0	12.0
72	35	46.3		60.5		12.0	
81	60	41.3	39.6	56.8	56.8	12.0	11.5
82	60	37.8		56.7		11.0	
91	85	38.5	39.8	54.9	55.0	11.0	11.0
92	85	41.0		55.0		11.0	
101	110	37.1	37.8	52.4	52.6	12.0	12.0
102	110	38.5		52.8		12.0	
111	210	34.0	34.3	50.4	50.0	11.0	11.0
112	210	34.6		49.6		11.0	

spectrum of over-aged conditions, the same type of notched specimen was used. A schematic drawing of the notch is shown in Fig. 9 . This specimen is similar in other details to the conventional specimen shown in Fig. 10. The stress concentration at the root of the given notch is approximately 3.2 (Ref. 14).

Experimental Procedure

Alternate-immersion tests were conducted on a total of 22 specimens in a 3-1/2-percent NaCl solution. The specimens were loaded to 92.5 or 97.5 percent of their notch strength (N.S.). The latter values were read off a plot of tensile strength versus notch strength based on the data obtained for five different over-aged conditions. These data are listed below:

Specimen Number	Over-Aging Treatment	N.S., ksi	Related T.S., ksi	N.S. Ratio, $\frac{\text{N.S.}}{\text{T.S.}}$
13*	2 hours at 250 F	112.5	80.2	1.40
23*	6 hours at 250 F	107.8	79.3	1.36
133	6 hours at 350 F	93.8	73.6	1.27
63	20 hours at 350 F	83.6	64.1	1.30
113	210 hours at 350 F	66.4	50.0	1.33

*Originated from same forging as other specimens

Each of the stress-corrosion specimens was strained in its testing frame (described in Ref. 1) by an amount which was determined with the help of the load versus strain curves for the above five specimens. The strain was measured by a 1/2-inch extensometer and read on the strain recorder of a Riehle tensile testing machine.

Results

The stress-corrosion results are shown plotted in Fig. 11. As there was no pronounced difference between the data obtained at 92.5 percent N.S.

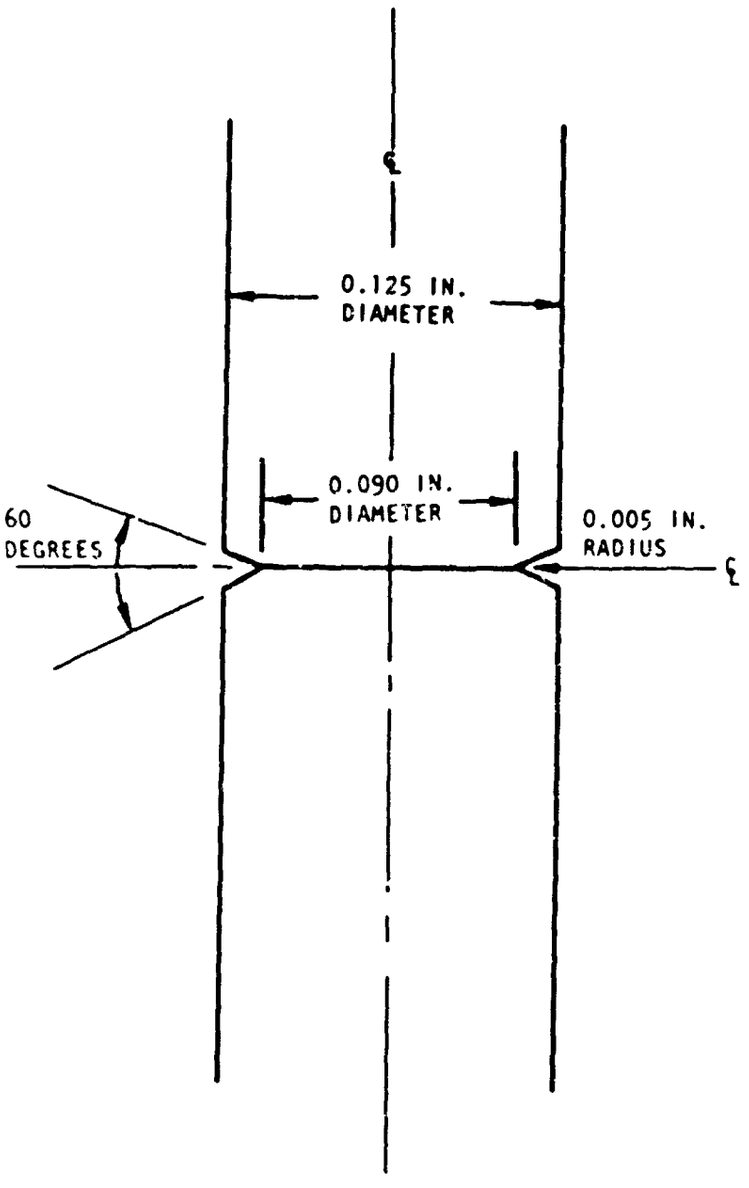

Figure 9. Notched 1/8-Inch Round Stress-Corrosion Specimen

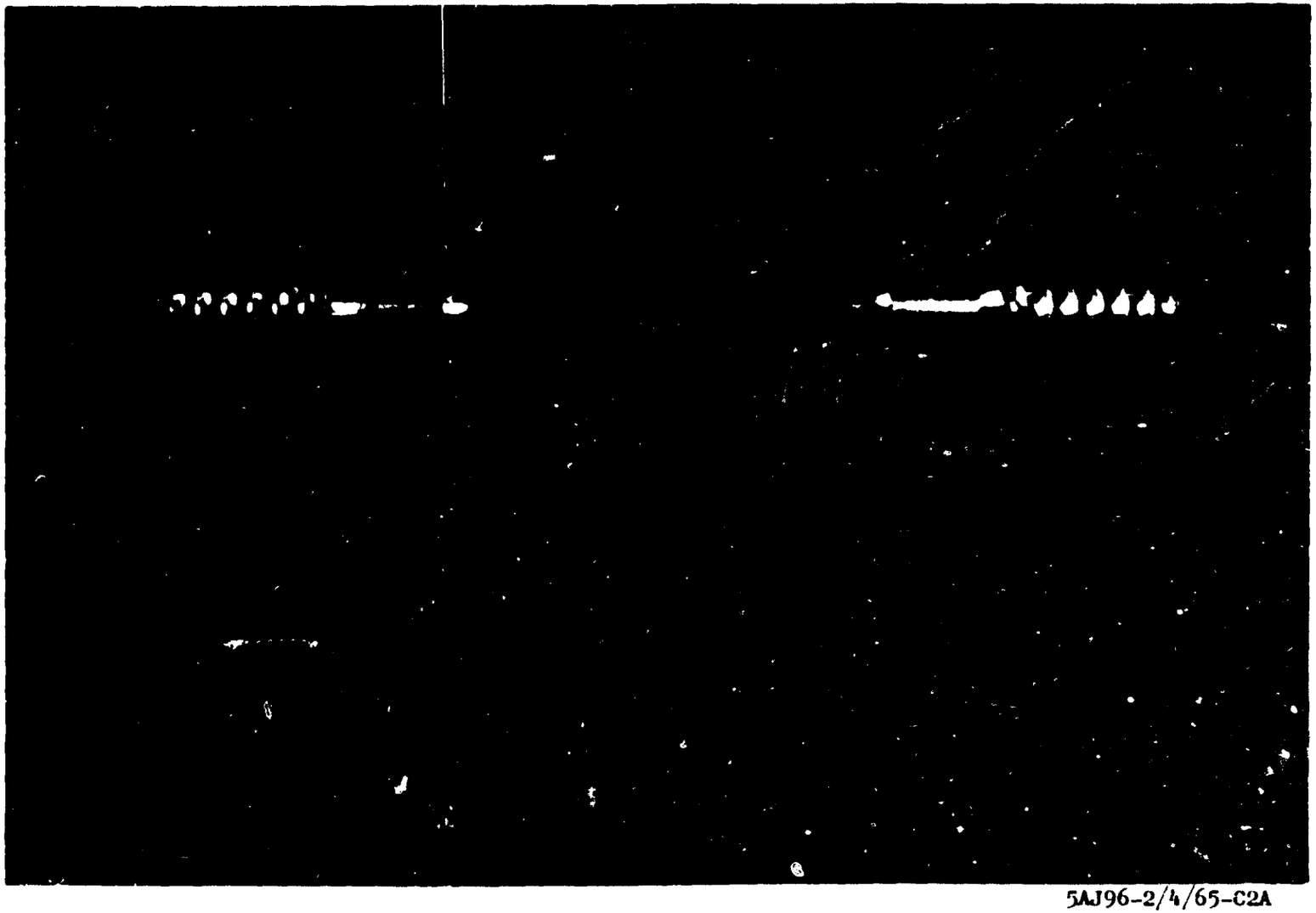

5AJ96-2/4/65-C2A

Figure 10. One-Eighth-Inch Round Stress-Corrosion Specimen

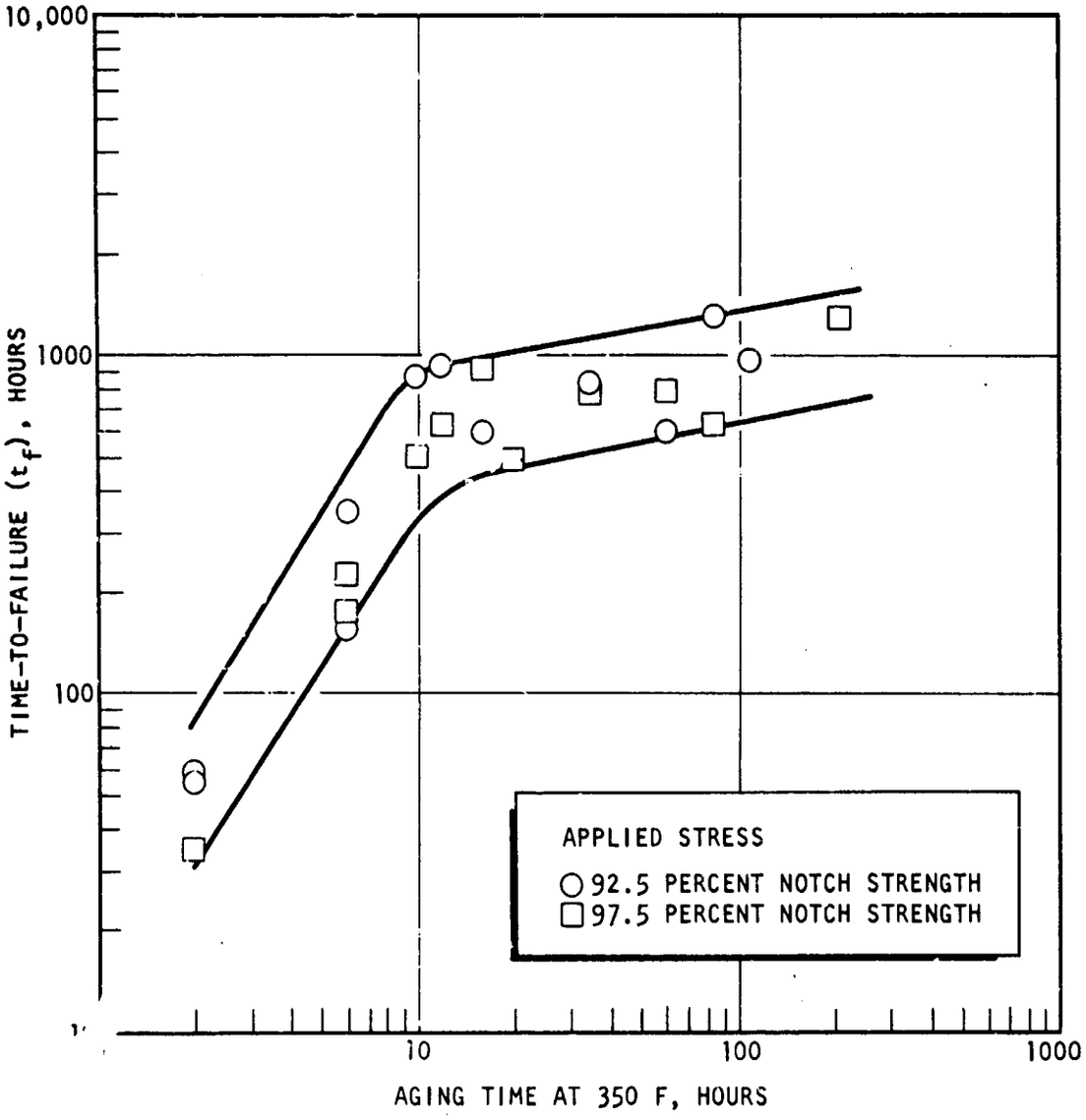

Figure 11. Stress-Corrosion Time-to-Failure of Over-Aged 7075 Plotted as a Function of Aging Time

and 97.5 percent N.S., all the points have been enclosed within a band, instead of being represented by two separate curves. It is observed that with increasing aging time (t_a), up to t_a = 10 hours, the time-to-failure (t_f) increases rapidly; while between t_a = 10 hours and t_a = 210 hours, the rate of increase in t_f is much more gradual. Thus, the t_f and yield-strength curves (Fig. 8) show similar changes in slope at t_a = 10 hours.

TEMPERATURE DEPENDENCE OF THE YIELD STRENGTH OF 7075

Various theories have been proposed, which predict the temperature variation of the yield strength of a precipitation hardening alloy. The temperature dependence, of course, is intimately related to the mode of deformation. One cutting theory (Ref. 15), wherein the flow stress is ascribed to the work done in forcing dislocations through the precipitates, predicts a 2/3-power dependence of the flow stress on absolute temperature. The equation which applies is:

$$\tau = \frac{U_o}{\nu} \left\{ 1 - \left[\frac{kT}{U_o} \ln \frac{\dot{\epsilon}_o}{\dot{\epsilon}} \right]^{2/3} \right\}$$

where τ is the flow stress, U_o is a potential energy barrier, ν is an activation volume, $\dot{\epsilon}_o$ and $\dot{\epsilon}$ are strain rates, T is absolute temperature, and k is Boltzmann's constant. The temperature dependence of the bypassing process, in which the flow stress is governed by the stress necessary to force dislocations between obstacles, has been considered by Orowan (Ref. 16). It was concluded that no temperature dependence will arise for particles of diameter greater than a few atom distances except through the variation of the elastic moduli with temperature.

To determine whether the deformation mechanisms do indeed differ in 7075-T6 and -T73, tensile tests have been conducted over the temperature range from -423 F to room temperature. If the G.P. zones in -T6 are sheared, and the particles in -T73 bypassed, then one might expect a $T^{2/3}$ dependence of τ(-T6) and a much smaller temperature dependence of τ(-T73).

EXPERIMENTAL PROCEDURE

The starting material was the same hand-forged 7075-T73 billet that was described in the previous section (page 9). An approximately 1-inch-thick longitudinal section was cut off the billet, re-solution heat treated

at 895 F for 2 hours, and then given a standard -T6 aging treatment. Half of the section was finally over-aged to the -T73 condition. Ten 1/4-inch-diameter by 4-inch-long tensile specimens were machined from each of the two tempers.

The tensile tests were conducted in duplicate at each of five temperatures: ambient, -50, -175, -300, and -423 F. The subambient temperature tests were performed with a 60,000-pound-capacity Baldwin Universal Tensile Machine. A crosshead speed of 0.02 in./min and a 1-inch strain-gage-type extensometer were used in these tests.

RESULTS AND DISCUSSION

The complete tensile data are presented in Table 4. The yield strengths (τ) from each pair of duplicate tests were averaged and are shown plotted against absolute temperature (T) in Fig. 12 . The quantity, $(\tau_o - \tau)$, where τ_o is the extrapolated yield strength at T = 0, has been plotted against T in Fig. 13. In view of the form of Eq. 1, the slope of the latter plot gives the exponential dependence of τ directly.

A least-squares fit of all the -T6 and -T73 data is seen in Fig. 13A to yield straight lines with slopes of 0.59 and 0.56, respectively. These values are in reasonable agreement with the theoretically predicted value of 0.67 for a shearing mechanism. Taking account of the curvature that can be observed at the high-temperature end of the -T6 and -T73 curves, and fitting only three points on each curve to straight lines (Fig. 13B), even better agreement is obtained between the experimental and theoretical slopes. The experimental values now bracket the 0.67 value: they are 0.71 (-T6) and 0.60 (-T73).

Thus, the data lead to the surprising conclusion that the deformation mechanisms are very similar in 7075-T6 and -T73. At low temperatures (<160 K), the data provide especially strong support for a shearing model.

TABLE 4

TENSILE DATA

Temperature, F	Specimen Number	Temper	Y.S. (0.2 Percent Offset), ksi	T.S., ksi	Elongation (1-in. G.L.), percent
Ambient	1	-T6	71.3	79.6	3
	2	-T6	70.7	79.6	4
	11	-T73	57.8	68.7	8
	12	-T73	58.7	69.2	7
-50	3	-T6	70.0	78.5	7
	4	-T6	71.2	79.1	5
	13	-T73	59.6	69.7	6
	14	-T73	60.1	67.1	5
-175	5	-T6	74.8	81.9	4
	6	-T6	74.0	81.8	4
	15	-T73	61.7	73.7	6
	16	-T73	62.6	75.5	6
-300	7	-T6	76.8	84.0	4
	8	-T6	78.8	82.7	4
	17	-T73	65.1	78.8	4
	18	-T73	67.5	76.2	4
-423	9	-T6	90.9	95.4	2
	10	-T6	91.6	93.2	2
	19	-T73	72.3	82.1	2
	20	-T73	72.4	85.8	3

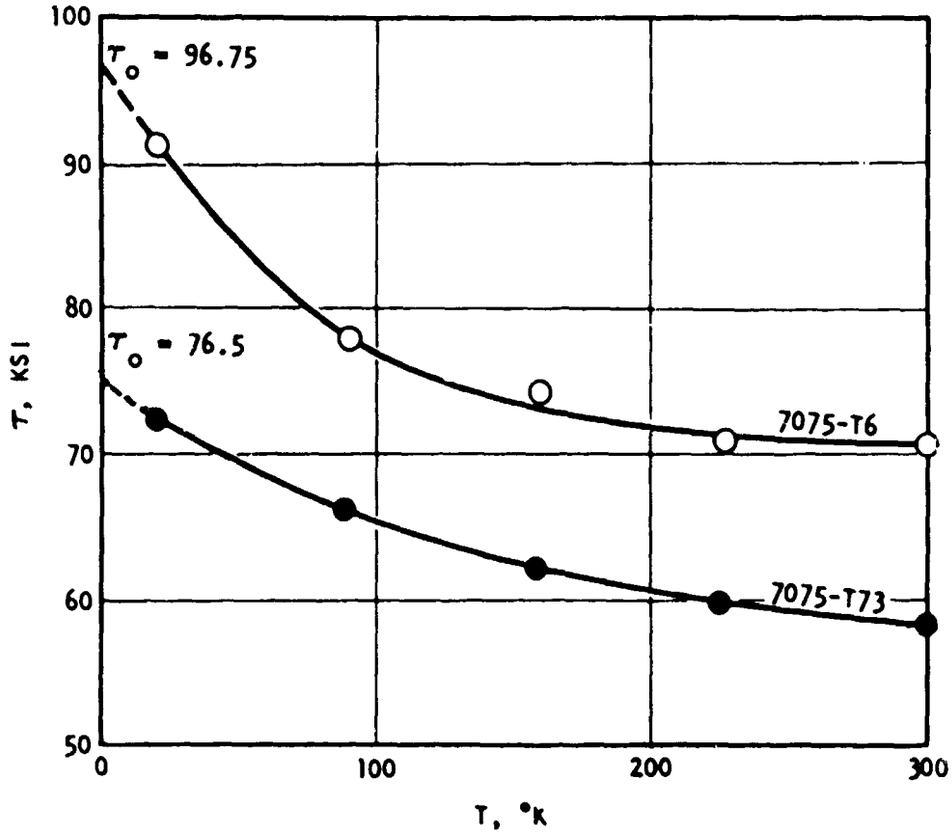

Figure 12. Plot Showing Yield Strength (τ) of 7075-T6 and -T73 as a Function of Temperature

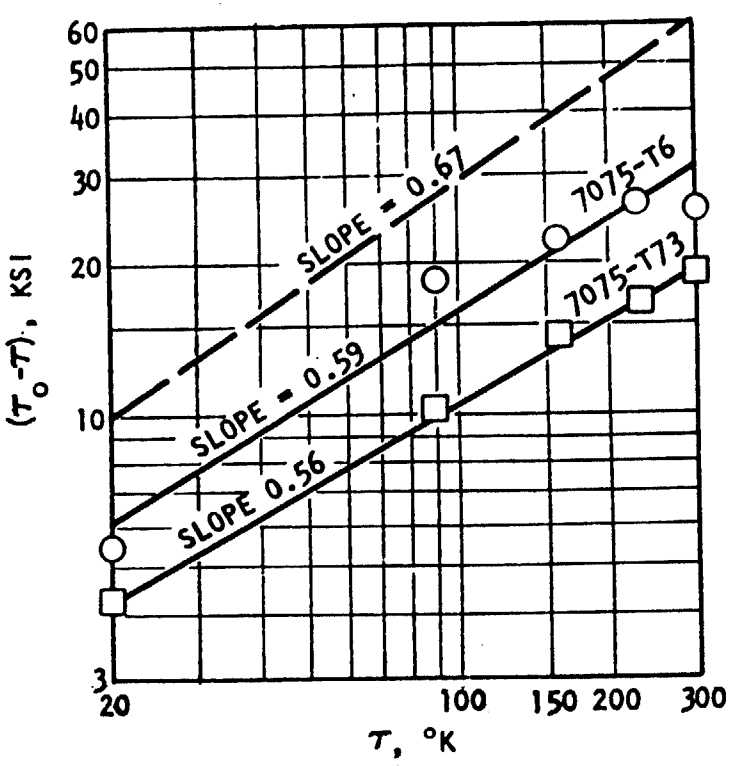

A. Least-Squares Fit Using All Data Points

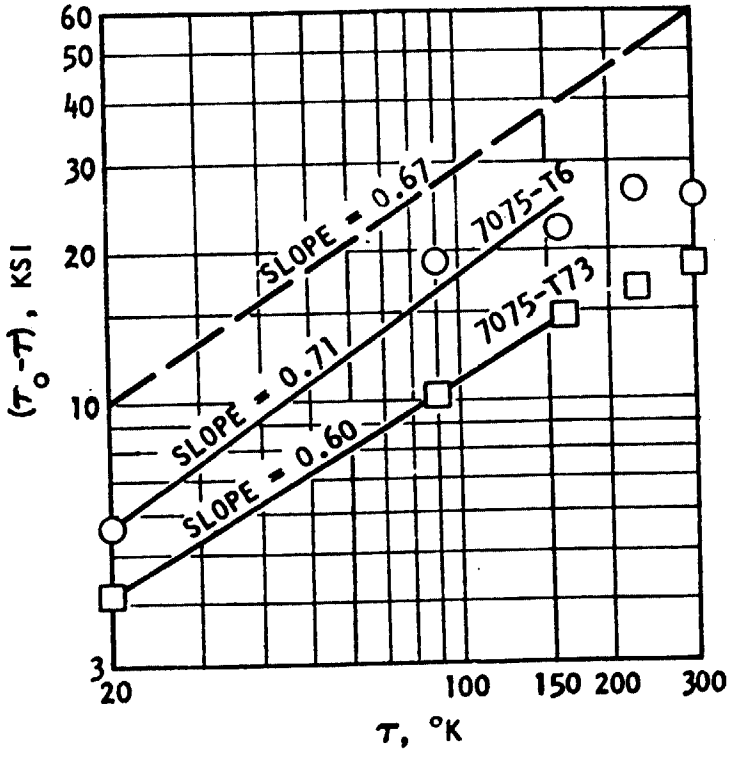

B. Least-Squares Fit Using Three Data Points Only

Figure 13. Plot of $(\tau_o - \tau)$ vs Absolute Temperature for 7075-T6 and -T73

At higher temperatures (>160 K), the mechanism(s) seems to be less dependent upon thermal activation.

A striking parallel exists between the present results and the results obtained by Byrne et al (Ref. 17) and Matsuura and Koda (Ref. 18) with Al-1.8 percent Cu crystals. These investigators measured the temperature dependence of the critical resolved shear stress (CRSS) over the temperature range from 4.2 to 373 K. A plot of CRSS against $T^{2/3}$ gave a straight line at temperatures <150 K and another straight line at higher temperatures. To explain these results, Byrne assumed that there were two types of barrier to plastic flow. One of the barriers was large and was effective at all temperatures of deformation. The other barrier was small and became ineffective in resisting dislocation motion below a critical temperature (150 K). It is interesting to note that the break in the -T6 and -T73 curves (Fig. 13) occurs at 158 K.

It is fully realized that polycrystalline samples are not as satisfactory as single crystals for testing theories of mechanical behavior. The reason for this is the diverse precipitate structures of grain boundaries and grain interiors. However, single crystals of the complex 7075 alloy are not available. Even single crystals of this alloy could not be considered ideal, because of the diversity of precipitate compositions and morphologies that is inherent in the alloy composition.

DISLOCATION MOBILITY MEASUREMENTS

Whether the stress concentration at the base of a notch will be relieved by plastic deformation or by mechanical fracture will depend on the density of mobile dislocations and the mobility of these dislocations. Difficulties arise when one attempts to measure these parameters. The problem of measuring the mobile dislocation density is especially formidable and the direct measurement of dislocation mobility (by etch pit techniques) is likewise difficult. Therefore following the example of other investigators (Ref. 19 through 24), recourse has been made to two indirect methods wherein one determines the exponential dependence (m) of the dislocation velocity (v) on the applied stress (τ):

$$v = \left(\frac{\tau}{\tau_o}\right)^m \tag{1}$$

The plastic strain rate can be expressed as:

$$\dot{\epsilon} = \vec{b}\, n\, v \tag{2}$$

where $\vec{b}$ is the Burgers vector and n is the density of mobile dislocations. A quantity known as strain-rate sensitivity, which we designate by $1/m'$, can be derived from Eq. 2 by differentiation.

$$\frac{1}{\text{strain-rate sensitivity}} = m' = \frac{d\ell n\dot{\epsilon}}{d\ell n\tau} = \frac{d\ell nv}{d\ell n\tau} + \frac{d\ell nn}{d\ell n\tau} \tag{3}$$

Since

$$m = \frac{d\ell nv}{d\ell n\tau}$$

from Eq. 1 , it is seen that:

$$m' = m + \frac{d\ell nn}{d\ell n\tau} \tag{4}$$

The parameter m, therefore, is identical with 1/strain-rate sensitivity, m', if the second term in Eq. 4 is negligible, i.e., if the mobile dislocation density does not change with stress.

The first method used to measure m involved tensile tests, in which the change in flow stress was determined as a function of strain rate. The second method consisted of stress-relaxation tests, in which the rate of decay of an applied stress was measured. Other investigations used these techniques; and they are briefly discussed below.

Johnston and Stein (Ref. 20) have calculated the strain-rate sensitivity of LiF and Fe-3 percent Si single crystals and Fe-3 percent Si polycrystals from the measured changes of flow stress with strain rate at various strains (see Eq. 3). From m' they determined m using Eq. 4 . To ensure that the second term in Eq. 4 was negligible, Johnston and Stein extrapolated the values of m' to a value of m'_0 at zero strain. The value of m'_0, so obtained, agreed very well with the values of m measured directly. In tensile experiments on tungsten single crystals, Schadler (Ref. 21) showed that m can be determined from strain-rate sensitivity measurements only at very low strain.

Hull and Noble (Ref. 22) used three indirect methods to arrive at m. The three methods were shown to give comparable results for single crystals of Fe-3-1/4 percent Si. These methods were: (1) measurement of the strain rate dependence of the flow stress, (2) measurement of the change in strain rate produced by an increment of load to a creeping specimen, and (3) measurement of the relaxation curves produced by stopping the tensile test of a plastically deforming specimen in an elastically hard machine. Assuming a constant density of mobile dislocations, m can be determined from the relaxation curve as follows. The elastic strain rate of the specimen and machine at time τ after the start of relaxation is given by:

$$\dot{\epsilon}_e = -\frac{1}{E}\frac{d\tau}{dt}$$

where τ is the stress at time t and E is the elastic constant of the specimen and machine. In the absence of an imposed strain rate, the plastic strain rate $\dot{\epsilon}_p$ is equal to the elastic strain rate:

$$\dot{\epsilon}_p = -\dot{\epsilon}_e = -\frac{1}{E}\frac{d\tau}{dt}$$

Thus from Eq. 1 and 2:

$$-\frac{1}{E}\frac{d\tau}{dt} = K\tau^m$$

where

$$K = \frac{\vec{b}\, n}{\tau_o^m}$$

Integrating gives:

$$\ell n\tau = \frac{1}{(1-m)}\ell n(1 + At) + \text{constant} \qquad (5)$$

m is obtained directly from a plot of $\ell n\tau$ vs ℓnt provided $At \gg 1$.

An empirical relationship similar to Eq. 5 was derived by Chang (Ref. 24) from stress relaxation data for a large number of crystalline solids:

$$\ell n\tau = \frac{1}{(1-m)}\ell nt + \text{constant} \qquad (5a)$$

The valid time range for Eq. 5a was from a few seconds after the start of relaxation to a few minutes. Using notched bend specimens, Chang applied small, varying stress pulses at a given level of strain. He obtained a parameter m_o, which he suggested might be of fundamental significance, by calculating an m value for each stress pulse (σ_o), and extrapolating these m values to $\sigma_o = 0$. The m_o parameter was shown to vary between 3 and 4 for a series of alkali halides and uranium carbide. No values of m_o were reported for metals.

Concerning the relative advantages of the strain-rate sensitivity and stress-relaxation methods, a change in the mobile dislocation density is less likely to occur with the latter method. This is especially true when a large change in strain rate is required to produce a measurable change in flow stress in the first method. Also, small changes in flow stress will lead to large errors in measurement. A third advantage of the stress-relaxation type of test is that machine transients are more nearly eliminated.

EXPERIMENTAL PROCEDURE

Strain-rate sensitivity (SRS) and stress-relaxation (SR) tests were carried out on 7075-T6 and -T73 specimens, taken either from the longitudinal or the short-transverse direction of the original forging.

Strain-Rate Sensitivity

The specimens for these measurements originated from the same -T73 hand forging as the specimens discussed in the two previous sections. A 1-inch-thick longitudinal section was re-solution heat treated at 895 F for 2-1/3 hours (total time) and then aged to the -T6 or -T73 condition. Tests were conducted two 7075-T6 specimens of different orientation, and on two -T73 specimens, also of different orientation. The specimens had the same configuration as shown in Fig. 10.

Strain was measured by means of Budd C12-IXI-M50 strain gages having a 0.060-inch gage length and temperature compensated for aluminum; the strain was recorded on a Hewlett-Packard XY recorder. The testing machine was a model TT-C Instron with zero suppression unit.

Three strain rates were used: 0.02, 0.05, and 0.10 in./in./min. The lowest rate was used initially in each test. A pushbutton selector on the Instron machine provided the same precise control as a single-speed, synchronous cross-head-drive system. A typical recording of strain versus time is reproduced in Fig. 14. With the zero suppression unit on the Instron, load readings could be made easily to the nearest 0.5 pound.

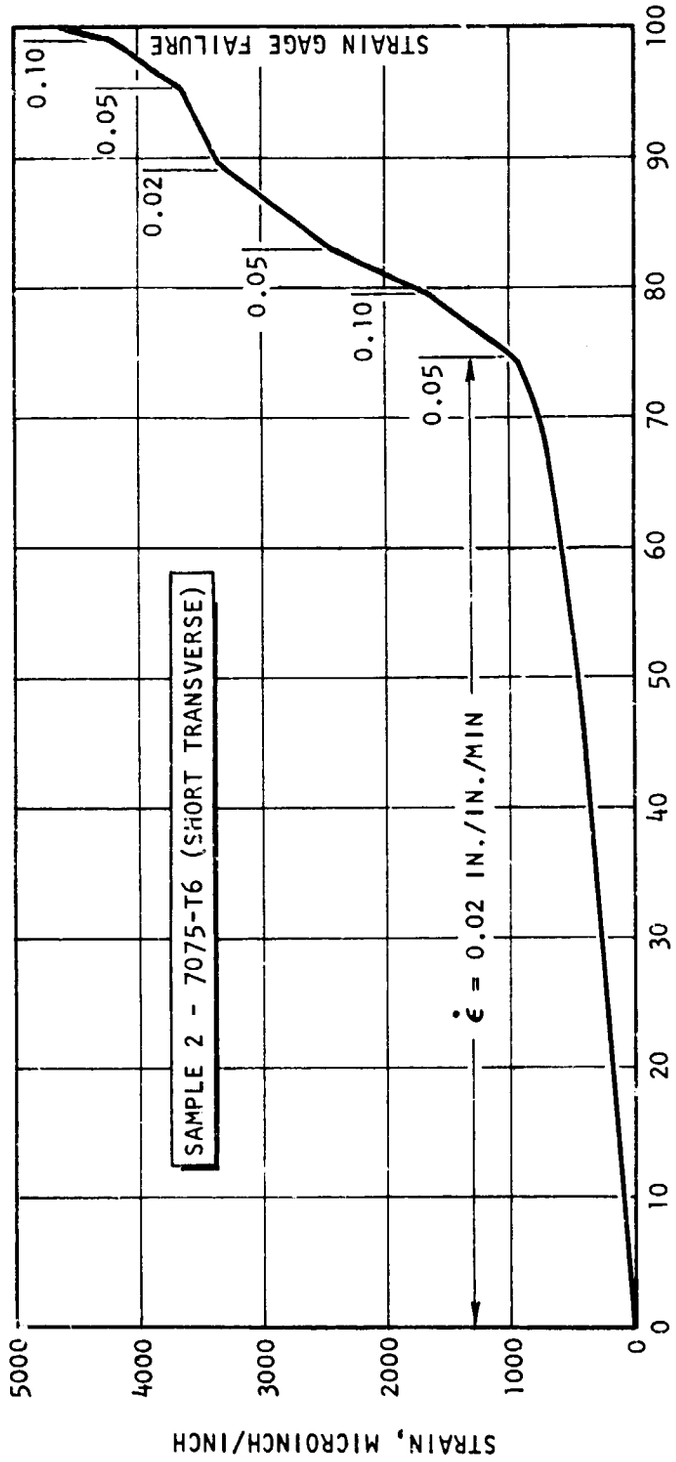

Figure 14. Typical Recording of Strain vs Time Obtained in Strain-Rate Sensitivity Test

Typical stress-strain curves for -T6 and -T73 are shown in Fig. 15 and 16, respectively. The changes in flow stress with strain rate are shown enlarged in the insets. m' values were calculated from the formula: $m' = d\ell n\dot{\epsilon}/d\ell n\tau$.

Stress Relaxation

The starting material was a 4- by 6- by 8-inch hand-forged -T73 billet conforming to Military Specification A-22771-B. The following composition was reported by the supplier: 5.50-percent Zn, 2.44-percent Mg, 1.66-percent Cu, 0.22-percent Fe, 0.19-percent Cr, 0.09-percent Si, 0.02-percent Mn, 0.02-percent Ti, and the balance Al. Representative properties (longitudinal direction) also reported by the supplier were 59,300-psi tensile yield strength and 71,150-psi ultimate tensile strength and an electrical conductivity of 39.5-percent IACS.

The -T6 and -T73 heat treatments were performed on re-solution heat treated (2 hours at furnace temperature of 895 F) 1-1/4-inch-thick longitudinal sections, which had been cut off the billet. Four V-notch bend specimens (Fig. 17, inset) were machined from each temper, two of longitudinal and two of short-transverse orientation. Four-point loading was used.

The initial loads applied to the specimens varied from ~30 to ~180 pounds. These loads were applied at a crosshead speed of 0.02 in./min. Following application of the load, the specimen was allowed to relax for ~2 hours at constant strain. A small stress pulse, which amounted to ~20 percent of the initial load, was applied at the end of the 2-hour period, at the same cross-head speed as the initial load. Relaxation of the pulse was recorded over a 5-minute time period. Values of m, however, were calculated from the slope of a log load versus log time plot over the time interval from 15 to 60 seconds. This interval was chosen such that machine transients would not be a factor and so that there would not be excessive time for the mobile dislocation density to change. Typical loading-relaxation-pulsing-relaxation curves have been reproduced in Fig. 17.

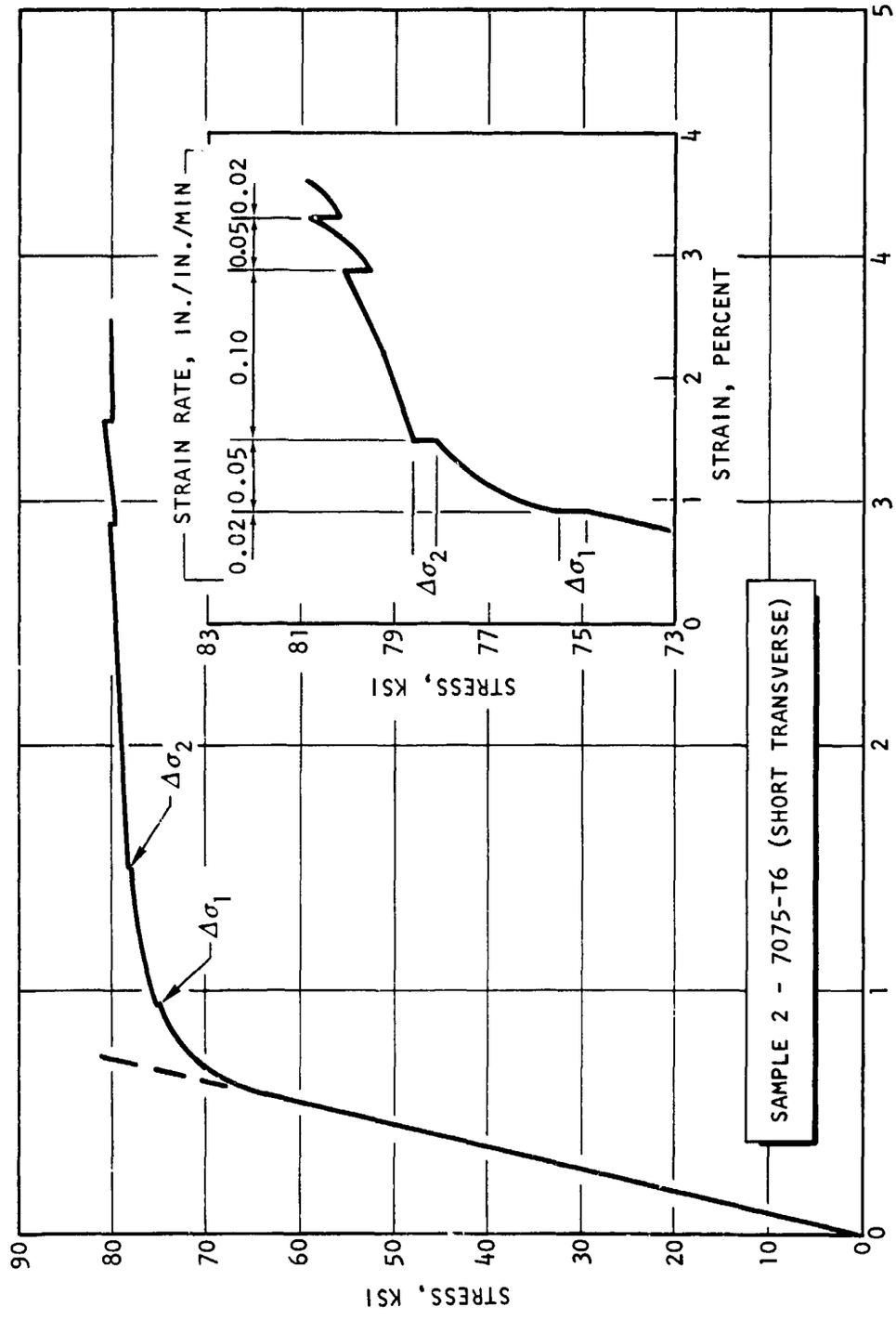

Figure 15. Typical Stress-Strain Curve Obtained for Short Transverse 7075-T6 Specimens in Strain-Rate Sensitivity Test

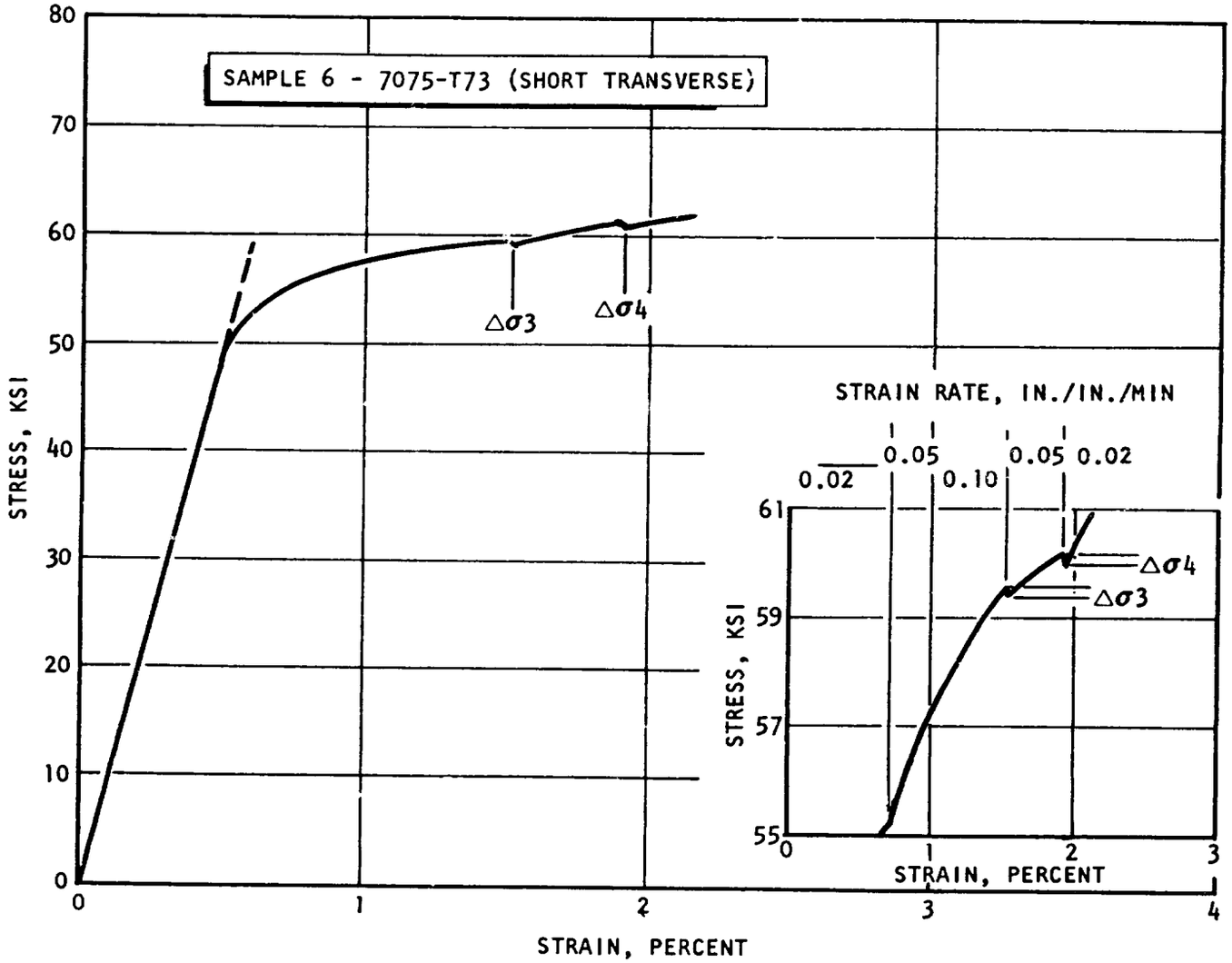

Figure 16. Typical Stress-Strain Curve Obtained for Short Transverse 7075-T73 Specimen in Strain-Rate Sensitivity Test

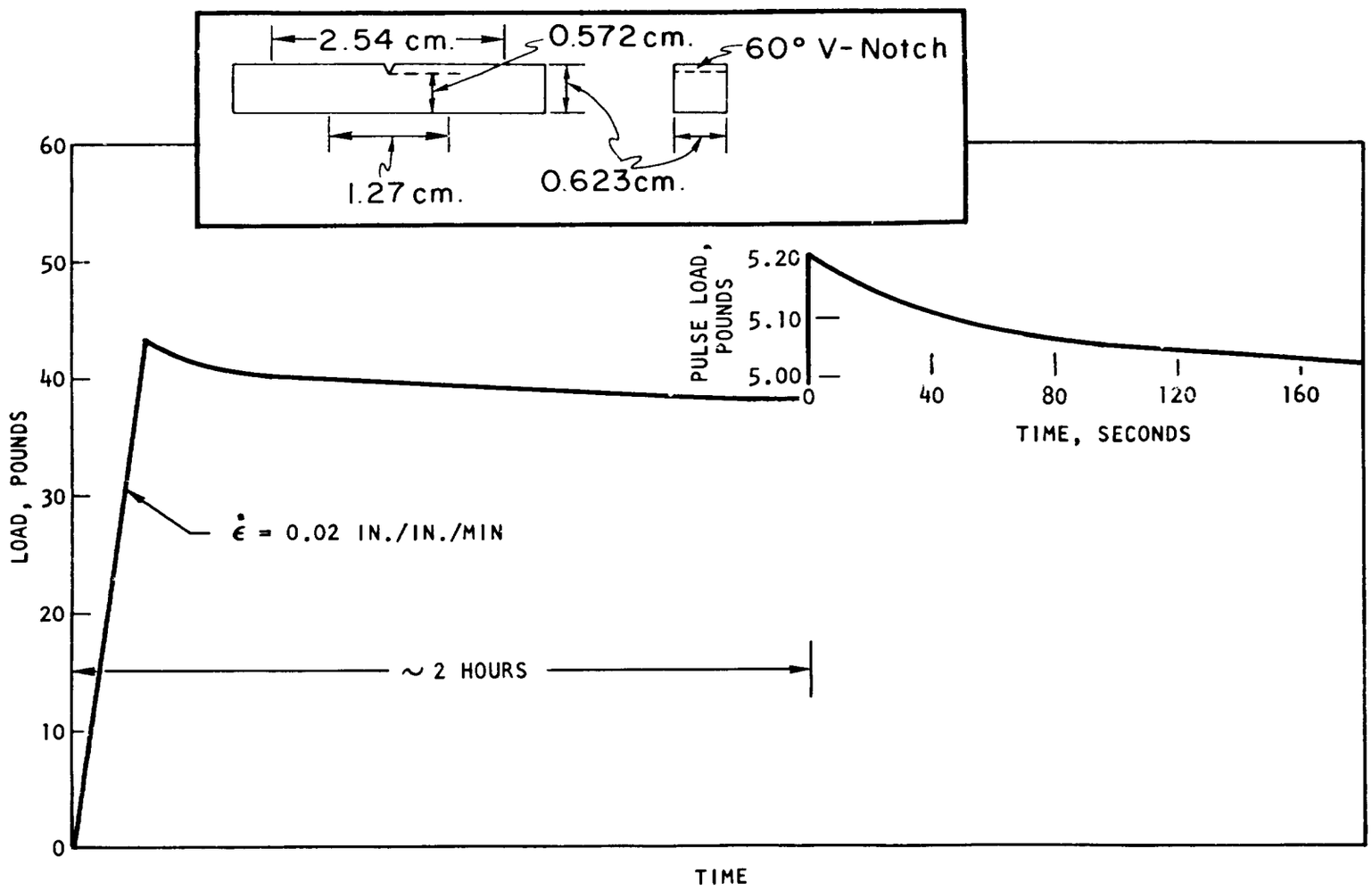

Figure 17. Typical Loading-Relaxation-Pulsing-Relaxation Curve

The first eight tests were conducted at total loads (initial load plus pulse) ranging from ~35 to ~70 pounds. Each of these tests was conducted on a different specimen. Following these tests, the specimens were stressed at higher levels. It will be pointed out in the Discussion section that strain aging was a complicating factor in the mobility measurements. Thus, it was imperative that the first test on a specimen be conducted at a low stress level, and subsequent tests on the same specimen, at higher stress levels, instead of vice versa.

RESULTS

Strain-Rate Sensitivity

The strain-rate sensitivity tests showed a pronounced difference in behavior of 7075-T6 and -T73 (Fig. 18). The value of m' for -T73 is observed to decrease from an initial value of 250 to 325, at a load ~100 pounds above the proportional limit, to a final value of 100 to 150 at a load some 100 pounds higher. The m' values for -T6 are fairly constant at a level of about 100. The longitudinal -T73 specimen tends to display a higher m' than the short-transverse specimen, but there is no apparent effect of orientation in the case of the -T6.

Stress Relaxation

The results of the stress-relaxation tests indicate a tendency for m to decrease abruptly at a certain load, thereafter remaining constant within experimental error (Fig. 19). The longitudinal -T6 specimen is the first to show this drop in m with increasing load and is closely followed by the longitudinal -T73 specimen. The m values for short-transverse -T6 and -T73 specimens remain below 60. Individual points have been plotted for the first eight tests only. A scatter band has been drawn to include the remaining results obtained at higher stress levels.

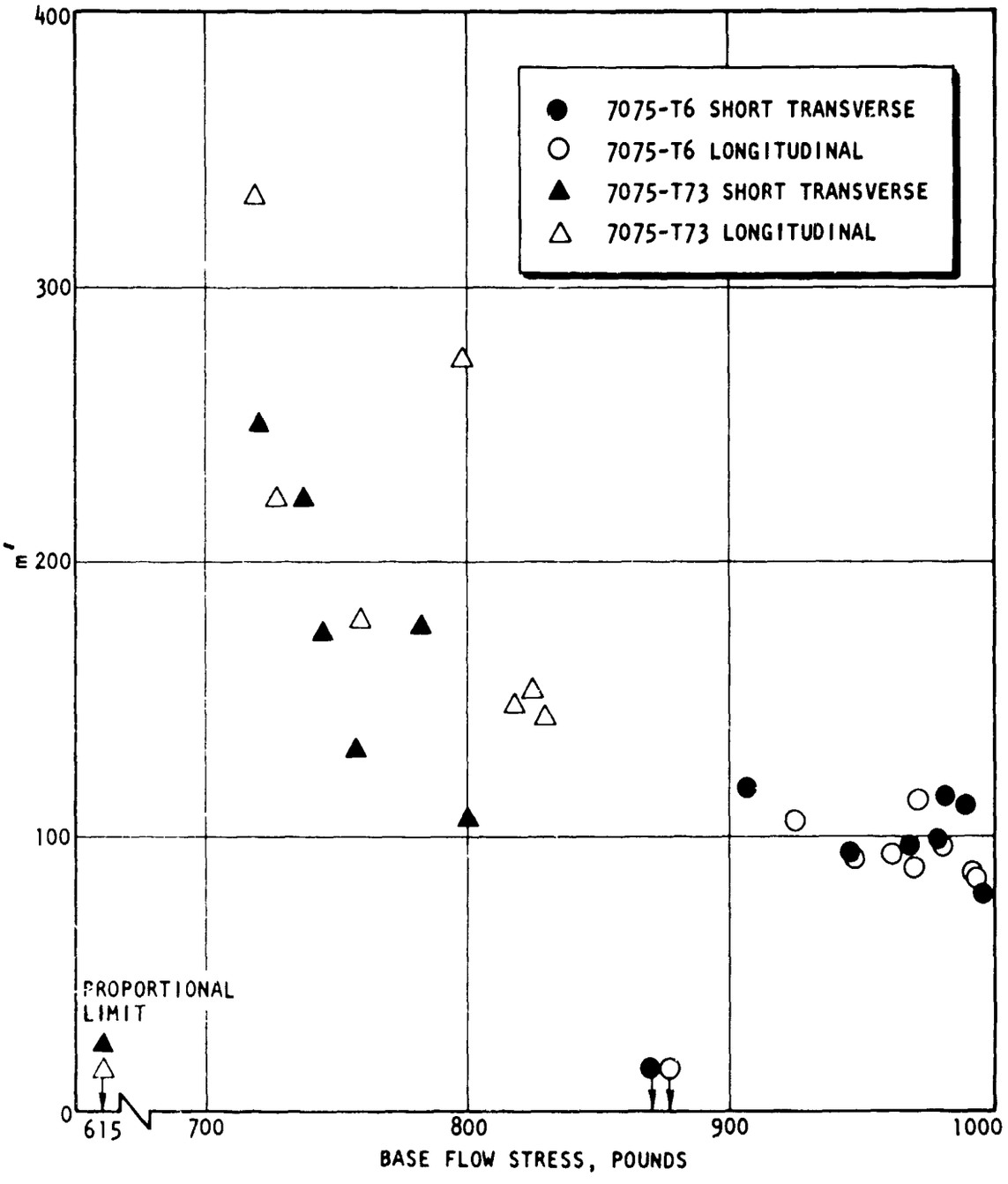

Figure 18. Plot of m'(= 1/Strain-Rate Sensitivity) vs Base Flow Stress for Two Orientations of 7075-T6 and -T73 Specimens

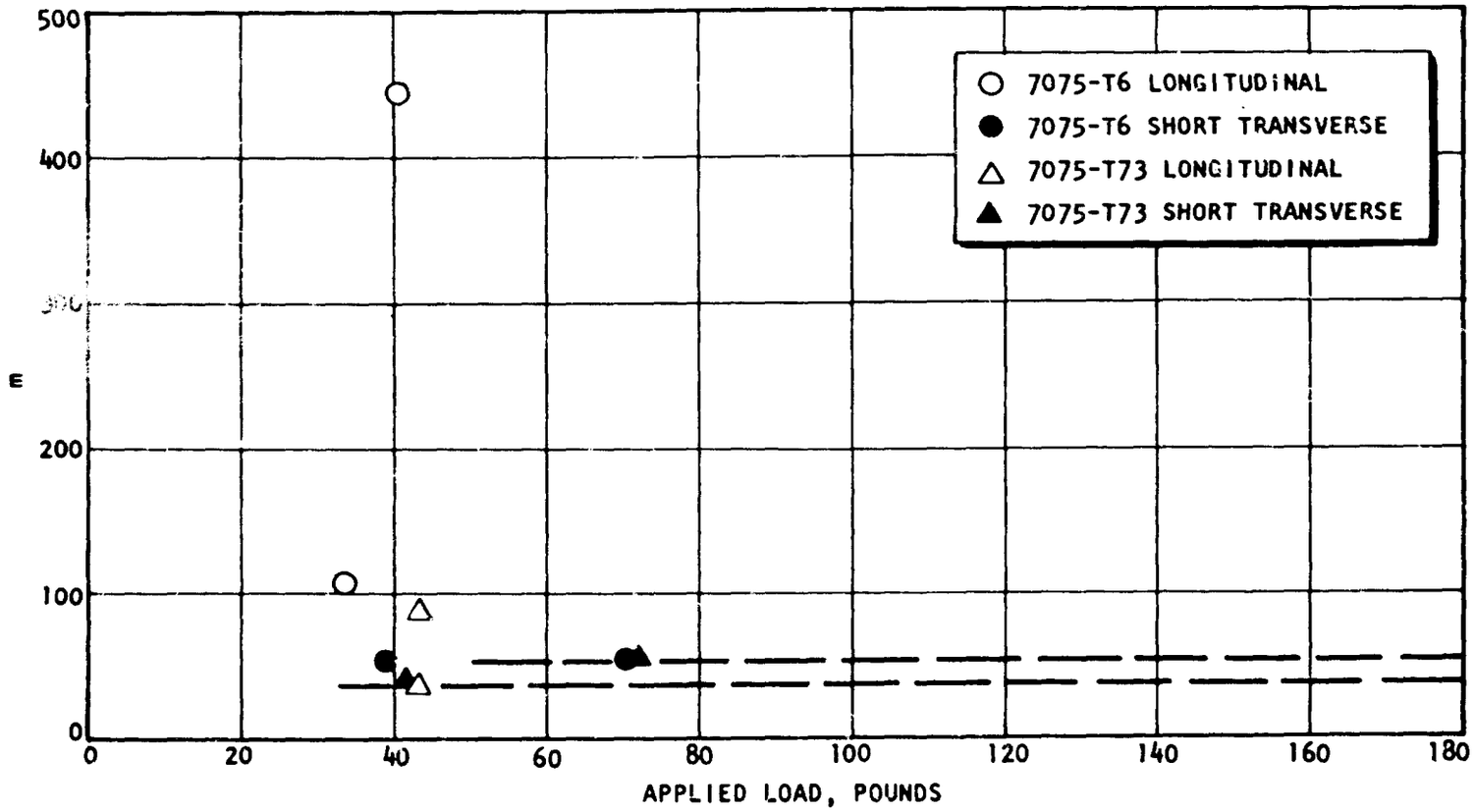

Figure 19. Plot of m vs Applied Load (Including Pulse) for Two Orientations of 7075-T6 and -T73 Specimens

DISCUSSION

The strain-rate sensitivity (SRS) measurements have demonstrated that a significant difference exists between the strain-rate sensitivity of 7075-T6 and -T73. This difference is most pronounced at low flow stresses and diminishes as strain hardening and strain aging progress in the -T73. Strain aging in -T73 was suggested by the presence of a yield drop in the stress-strain curve of a twice loaded sample (the first curve obtained did not show a drop). A similar yield drop was found during the second loading of a -T6 sample. Earlier work (Ref. 1 and 25) indicated that -T6 is very susceptible to strain aging while -T73 is not susceptible at all; however, a hard tensile testing machine was not used in that work. The present SRS results, considered together with the stress-relaxation (SR) data (Fig. 19), which yielded a high value of m (7075-T6) at sufficiently low loads, also indicate that strain aging proceeds rapidly in this temper. The full effect of strain aging on the strain-rate sensitivity is observed at a load which is only 35 pounds in excess of the measurable proportional limit (Fig. 18). A strain hardening exponent of ~0.07 was calculated for both -T6 and -T73 tempers from the true stress-true strain data appearing in Ref. 26 . Thus, the large difference between the strain-rate sensitivities of -T6 and -T73 at low flow stresses can be attributed mainly to the different strain aging propensities of these tempers.

Because of the obvious change taking place in the mobile dislocation density in -T73 as a result of strain hardening and strain aging, m cannot be equated with m' in the relation $m' = m + d\ell nn/d\ell n\tau$, even at the lowest flow stress, which was ~100 pounds above the proportional limit. Moreover, insufficient data were obtained to permit an accurate extrapolation of m' to zero strain (Ref. 19). The SRS results indicate only that m(-T73, longitudinal) >330 and m(-T73, short transverse) >250. The rapid onset of strain aging in the -T6 temper does not permit any estimate to be made of m(-T6). The limited SR data show that m(-T6, longitudinal) can be quite high (445), especially when compared to typical values (32 to 55) reported for some body centered cubic metals (Ref. 27). Thus, although the present results have not produced reliable estimates of m, they have served to emphasize the importance of

strain aging in the deformation of 7075-T6 and -T73. The determination of m values which truly approximate directly determined m values must await the performance of a much larger number of tests, especially at low applied stresses where strain-aging effects are negligible and the population of mobile dislocations is likely to remain constant. The effects due to strain aging can be eliminated by testing at a low enough temperature.

Although not as prominent as the difference in m' between the -T6 and -T73 tempers, a difference in m' and m also seems to be associated with orientation differences. This difference can be seen in Fig. 18, where m'(longitudinal -T73) tends to be higher than m'(short transverse -T73). It is also suggested in Fig. 19, where three of the four longitudinal specimens are seen to have m's of about 100 or greater, while the m's of all four short-transverse specimens vary between 40 and 60. The difference between the two -T6 orientations is apparently masked by strain aging effects in the SRS tests but not in the SR tests.

The present SRS results disagree in some important respects with, or complement, the recently reported results of others. Holt et al. (Ref. 28) have found that the flow stress of 7075-T6 tested in compression is unaffected by changes in strain rate over the range from 3.0×10^{-2} to 5.6×10^{2} in./in./sec. These strain rates are several orders of magnitude higher than the present ones (3.3×10^{-4} to 1.65×10^{-3} in./in./sec), which probably explains the different results. Strain aging is less likely to be a factor at the higher strain rates. The present results have shown that strain aging sets in early and is virtually complete soon after the proportional limit of -T6 has been reached. The high m(-T6) values obtained in two of the SR tests are in better agreement than the SRS data with Holt's results. Presumably there was little if any strain aging in those two tests, partly as a result of the high strain rate operating at the base of a notch.

Brummer et al. (Ref. 26) have carried out SRS tests on 7075-T6 and -T73 using strain rates of 7.3×10^{-3} and 7.3×10^{-4} in./in./sec. The latter value falls within the lower end of the range used in the present study; thus Brummer's rates are well below the range used by Holt (Ref. 28). The

results were quite unusual. Short-transverse -T6 specimens showed the expected increase in flow stress with increasing strain rate. Longitudinal -T6 and short-transverse -T73 specimens, however, showed a decrease in flow stress with an increase in strain rate. This decrease was attributed to "the pinning of dislocations by diffusion of solute atoms which can occur to a greater extent at the slower strain rate than at the higher. The decrease arising from the aging effect is greater than the increase to be expected because in any real material only finite lengths of dislocation can be activated by a given stress." Thus strain aging is suspected to play a role in Brummer's results. In the present study, both the -T6 and -T73 tempers, in both the short-transverse and longitudinal orientations, showed the anticipated increase in flow stress with increasing strain rate. The reason for the difference in results is not clear at the present time, especially since comparable strain rates were used.

INTERNAL FRICTION MEASUREMENTS

The results of preliminary amplitude-dependent internal friction measurements on different heat-treated conditions of 7075 were presented in the last Final Report (Ref. 1). The purpose of these measurements was to obtain information concerning the magnitude of dislocation-precipitate interactions, dislocation density, and the number of pinning points. According to the Granato-Lücke theory, the damping (Δ) is given by:

$$\Delta \sim \rho \, l^4 \tag{6}$$

where ρ is the dislocation density and l is the average free loop length or average length of dislocation segment between pinning points. This relation has been verified for several materials. An estimate of the binding energy between dislocations and pinning points can be determined from values of the breakaway stress.

The previous results (Ref. 1) were similar for the four conditions studied: an under-aged (relative to -T6) specimen (6 hours at 250 F), a -T6 specimen, and two over-aged (also relative to -T6) specimens (4 hours at 350 F and -T73). Sharp dislocation breakaway occurred at strains equal to $\sim 6 \times 10^{-6}$. A very slight hysteresis in the measurements was observed, but no aging effects were noted following the experiments that would suggest motion of pinning points back to the dislocations (or vice versa).

EXPERIMENTAL PROCEDURE

Five additional under-aged conditions, comprising a total of seven specimens, were investigated during this report period. The various heat treatments are summarized in Table 5.

Specimens 9, 10, and 11 received identical heat treatments: they were solution heat treated and rapidly quenched in iced brine, with no subsequent aging treatment. Specimens 5 to 8 were solution heat treated, quenched into water at room temperature, and finally aged at 250 F for times varying from 1/2 to 2 hours. The seven specimens originated from the same 7075 forging as the four specimens tested previously.

TABLE 5

HEAT TREATMENT SUMMARY

Specimen No.	Heat Treatment	Remarks
5	Solution heat treatment (SHT) (895 F, 1 hour), water quench (WQ); aged at 250 F for 2 hours	
6	SHT, WQ, aged at 250 F for 1-1/2 hours	
7	SHT, WQ, aged at 250 F for 1 hour	
8	SHT, WQ, aged at 250 F for 1/2 hour	
9	SHT (895 F, 1 hour), iced brine quench (16 F)	At ambient temperature for 20 minutes prior to measurements
10	Same as for No. 9	At ambient temperature for 20 hours prior to measurements
11	Same as for No. 9	At ambient temperature for 24 hours prior to measurements

The internal friction was measured using an apparatus similar to that described by Thompson and Glass (Ref. 29). Measurements were performed in a vacuum of approximately 10^{-1} torr. In this technique, the sample is held at a fixed amplitude of oscillation by an electronic servo-type amplifier in a regenerative loop. It can be shown (Ref. 29) that at sample resonance, the sample damping is directly proportional to the force necessary to sustain any preset level of oscillation; consequently, damping measurements may be made simply by measuring the current in the electromagnetic drive coil in this case. Such measurements are calibrated in terms of the standard methods for measurement of the logarithmic decrement.

RESULTS AND DISCUSSION

The newly obtained damping curves are observed in Fig. 20 to fall into two groups. The first group, representing the solution treated-and-unaged samples, lies at approximately three times the damping level of the solution treated-and-aged samples. There is a perceptible trend within the second group toward lower damping with longer aging time; only the curve for sample 5 occurs out of sequence. The most highly aged samples, which were tested previously, showed the lowest damping, the average value being about twice background ($\Delta_B = 4 \times 10^{-6}$). Thus, the amplitude-independent damping decreases by an order of magnitude or more, as the aging time at 250 F increases from 0 to 6 hours.

Only the curves for the solution treated-and-unaged samples show an amplitude dependent part, rather than sharp breakaway, at the high strain-amplitude end of the strain range. A Granato-Lücke plot of the amplitude-dependent data, which will be discussed below, indicates that the breakaway law (hysteretic losses) is operative for these curves.

It is implied in Eq. 6 that the number of pinning points, and thus the kinetics of the precipitation process, can be determined from the three groups of damping curves in Fig. 20. Although the available data do not permit an estimate to be made of absolute numbers of pinning points, they do enable estimates to be made of relative numbers. In the following analysis, an average aging time and an average amplitude-independent damping value will be used to represent each of the upper two groups of curves; the third group will be subdivided into two parts, the under-aged specimen in this group being treated individually. The average times and damping values are listed in Table 6.

The numbers of pinning points to be calculated will be relative to the unaged condition, which is assumed to contain 0 pins.

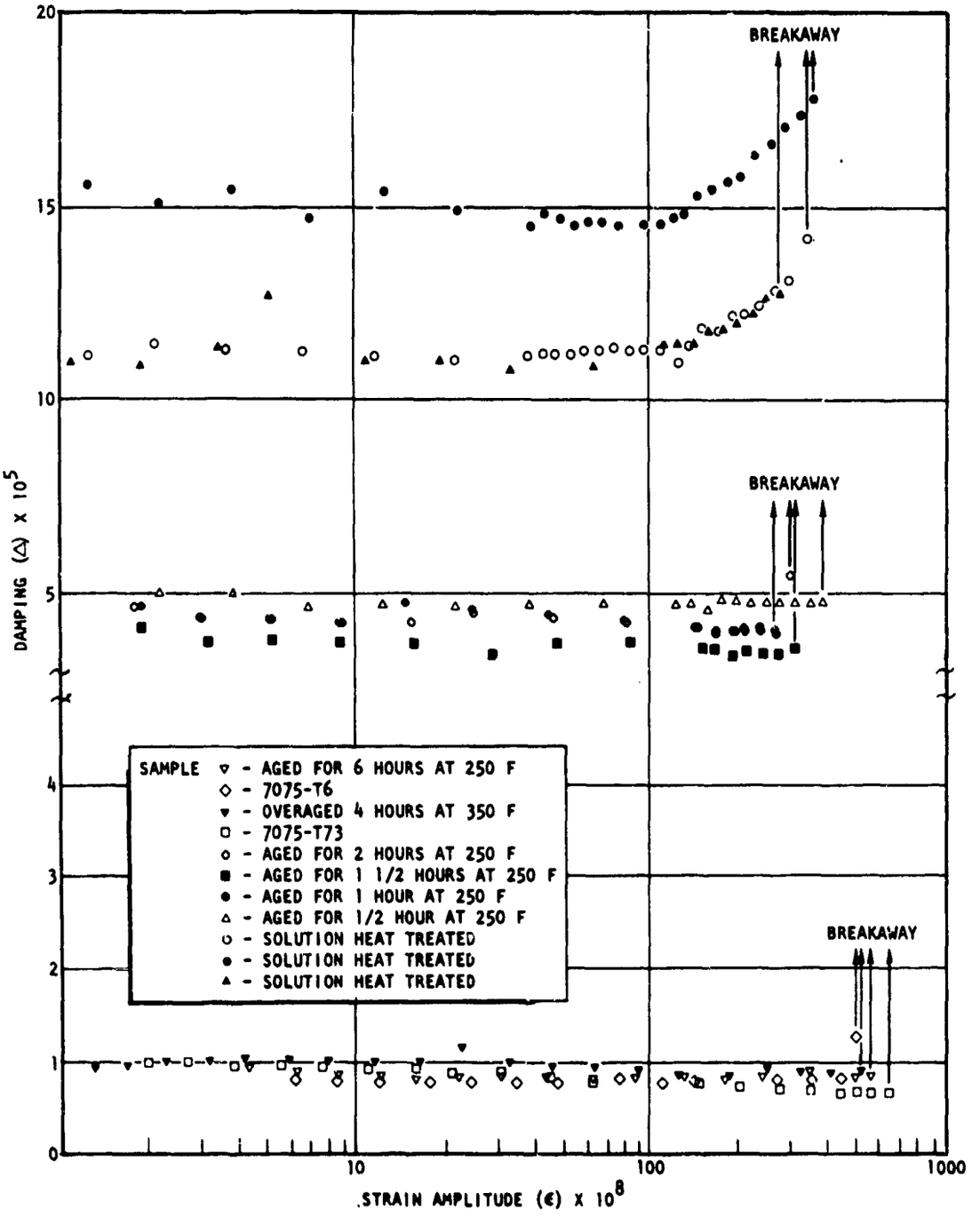

Figure 20. Damping vs Strain Amplitude for Variously Heat Tested Conditions of 7075

TABLE 6

AGING TIMES AND DAMPING VALUES

Sample	Average Aging Time, hours at 250 F	Average Amplitude-Independent Damping, $\Delta \times 10^5$
9, 10, 11	0	12.5
5, 6, 7, 8	1.25	4.25
1	6.0	0.85
2, 3, 4	24.0+	0.9

We define a quantity, Z, so that

$$Z = \frac{\Delta_t - \Delta_B}{\Delta_o - \Delta_B} = \frac{\ell_t^4}{\ell_o^4} \tag{7}$$

where Δ_t is the average amplitude-independent damping associated with average aging time t, Δ_B is the background damping, Δ_o is the damping at t = 0, and ℓ_o and ℓ_t are the average lengths of dislocation segment between pinning points at times 0 and t, respectively. Since

$$\ell_t = \frac{\ell_o}{1+n}$$

where n is the number of pinning points formed during aging, Eq. 7 can be rewritten as

$$Z = \frac{\Delta_t - \Delta_B}{\Delta_o - \Delta_B} = \frac{1}{(1+n)^4}$$

Thus,

$$n = Z^{-1/4} - 1$$

The calculated values of n are shown plotted against aging time in Fig. 21. A log-log scale has been used for convenience in depicting the slope.

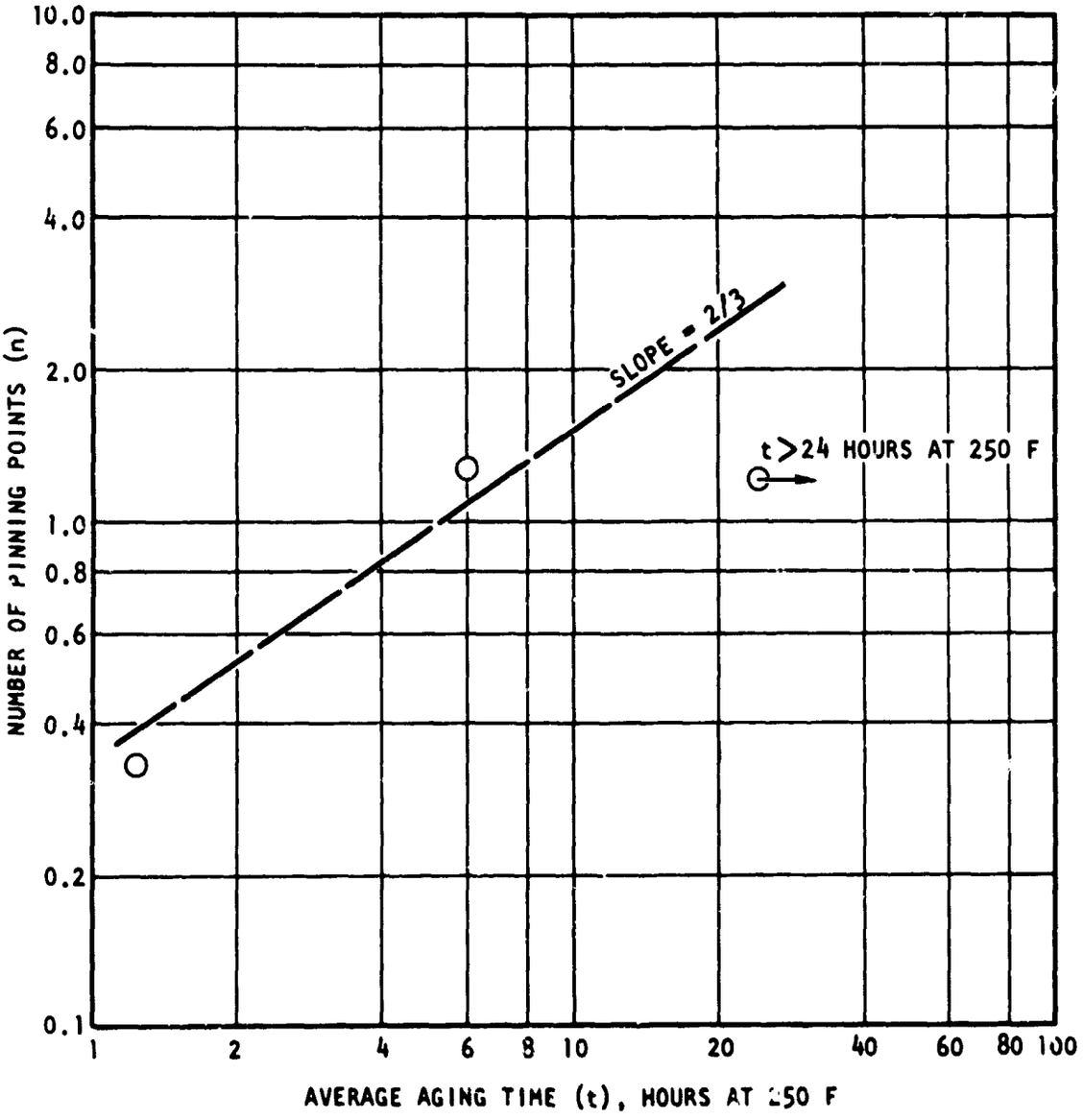

Figure 21. Number of Pinning Points Plotted as a Function of Aging Time

If the rate at which dislocations are pinned is governed by a diffusion mechanism, i.e., diffusion of the pinners to the dislocations, then the plot of log n vs log t should have a slope of 2/3. This conclusion follows from the Cottrell-Bilby theory of strain aging (Ref. 30). According to this theory, the fraction of original solute which has segregated to dislocations in time t can be written as

$$f = \alpha \rho (A\ Dt/kT)^{2/3} \qquad (8)$$

where

α = $3(\pi/2)^{1/2}$

ρ = dislocation density

A = Cottrell interaction constant, which is a measure of the binding energy between a solute atom and a dislocation

k = Boltzmann's constant

T = absolute temperature

A/kT = a measure of the range of interaction between solute atom and dislocation

A straight line having a slope of 2/3 has been drawn between the first two experimental points. These points fit the line quite well, which indicates that the Cottrell-Bilby law is obeyed for aging times up to 6 hours.

For longer aging times (>24 hours), the experimental point deviates from the line in the expected manner. Equation 8 is not valid for later stages of aging because it does not take into account solute depletion from the lattice.

A Granato-Lücke plot (Ref. 31) has been made using the data obtained from one of the unaged specimens (No. 10). The reasons for making such a plot were twofold: (1) to determine if the breakaway law was operative, and, if it was, (2) to obtain a measure of the breakaway stress. According to Granato and Lücke, dislocation hysteresis is due to the stress-induced breakaway of dislocation segments from impurity atoms to which they were locked, followed by the irreversible collapse of the long loops thus formed.

Two segments ℓ_1 and ℓ_2 will break loose from an impurity atom at A when

the applied force f_τ exceeds the binding force of the impurity atom to the dislocation, f_b, i.e., when

$$f_\tau > f_b$$

or $$\tau b\,(\ell_1 + \ell_2) > f_b$$

$$\tau > \frac{f_b}{b(\ell_1+\ell_2)}$$

where τ is the breakaway stress and b is the Burgers vector. Granato and Lücke (Ref. 31) have shown that if the breakaway law is operative, a plot of log $\epsilon(\Delta - \Delta_{AI})$ vs $1/\epsilon$ (where Δ is the amplitude-dependent and Δ_{AI} the amplitude- independent part of the damping) should yield a straight line of slope $\pi\,\tau/4G$ (where G is the shear modulus). The G-L plot for Specimen No. 10 is a straight line, as shown in Fig. 22. The slope of this line is 2.9×10^{-6}, so that if $G = 2.7 \times 10^{11}$ dyne/cm^2 (3.9×10^6 psi) (Ref. 32), τ is found to be $2.9 \times 10^{-6} \times 2.7 \times 10^{11} \times 4/\pi = 1 \times 10^6$ dyne/cm^2. The breakaway strain calculated from this value of τ is

$$\epsilon = \frac{\tau}{G} = \frac{10.0 \times 10^5}{2.7 \times 10^{11}} = 3.7 \times 10^{-6}$$

which is consistent with the highest measured strain (3.55×10^{-6}) that the instrument was capable of producing. If a loop length, $\ell \sim 10^{-5}$ cm, is assumed, a breakaway force, f, can be calculated as follows:

$$f = \tau\, b\, \ell$$

$$= 10^6 \frac{\text{dynes}}{\text{cm}^2}\,(2.8 \times 10^{-8}\ \text{cm})(10^{-5}\ \text{cm})$$

$$= 2.8 \times 10^{-7}\ \text{dynes}$$

It is of interest to note that the breakaway stress which has been calculated is several orders of magnitude less than the macroscopic yield strength for solution treated-and-unaged 7075 (1.4×10^9 dyne/cm^2 or 20,000 psi).

The internal friction measurements which have been conducted to date point to this technique as being an extremely useful tool for studying the aging kinetics in the complex 7075 alloy. The limited data reported in this section have been shown to support the Cottrell-Bilby model for strain aging and the Granato-Lücke model for dislocation breakaway. Thus, there is encouragement that additional damping measurements could provide insight into the diffusion mechanisms which must eventually affect the mechanical and stress-corrosion behavior of the 7075 alloy. The ability of excess vacancies to influence the stress-corrosion resistance of 7075 has recently been established (Ref. 33). The manner in which they exert this influence could well be elucidated through diffusion studies using internal friction methods.

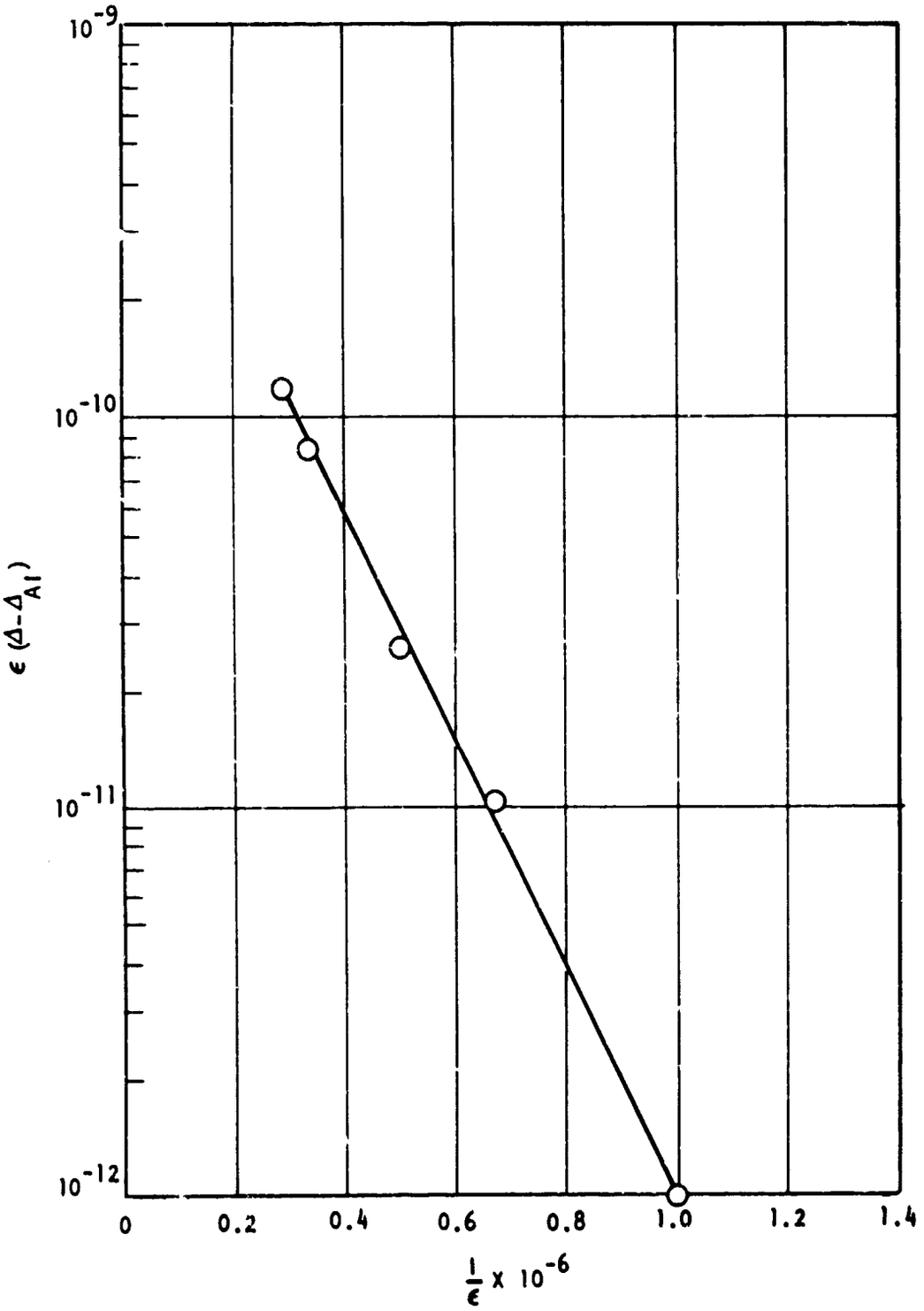

Figure 22. Granato-Lücke Plot for Solution Heat Treated 7075

EFFECT OF TENSILE DEFORMATION AND HIGH APPLIED STRESSES ON THE STRESS-CORROSION RESISTANCE OF 7075-T73

Following an experiment designed to determine the effect of prior tensile deformation on the stress-corrosion susceptibility of 7075-T6, a similar experiment was conducted on 7075-T73 (Ref. 25). The results were found to be dissimilar for the two tempers. The susceptibility of the -T6 increased with increasing predeformation, whereas the predeformation had no perceptible effect in the case of the -T73. Because there was considerable scatter in the limited number of tests that were run on the -T73, and because the -T73 had unexpectedly low stress-corrosion resistance in the undeformed state, the tests were repeated on material having better stress-corrosion resistance.

Another experiment performed in the last contract period was repeated because of the low stress-corrosion resistance of the -T73 control specimens, and because of the unusual nature of the results. In that experiment, the stress-corrosion time-to-failure increased as the applied stress was increased from 75 percent of the yield strength to 98 percent of the tensile strength. Seven tests were conducted at the 75 percent-of-yield stress level, but only one test was conducted at each of four stress levels above yield.

EXPERIMENTAL PROCEDURE

The procedures were the same as the ones used previously (Ref. 1 and 25).

In the tensile deformation experiment, four -T73 specimens were subjected to alternate-immersion tests in a 3-1/2-percent aqueous NaCl solution, after being plastically deformed to different stress levels. The specimens were loaded in their stress-corrosion frames to 75 percent of their post-deformation yield strength. The post-deformation yield strengths were measured on a separate group of -T73 specimens, which received the same deformation as the stress-corrosion specimens. The -T73 tensile and stress-corrosion specimens were 1/8-inch rounds. The deformation stresses and the post-deformation yield strengths are presented in Table 7.

TABLE 7

PRIOR DEFORMATIONS RECEIVED BY 7075-T73 STRESS-CORROSION SPECIMENS AND RESULTANT YIELD STRENGTHS

Specimen No.	Deformation Stress, psi	Post-Deformation Yield Strength (0.2 percent offset), psi
2	66,000	66,950
4	68,000	68,180
6	70,000	69,400
8	71,200	70,130
9, 10 (controls)	Undeformed	64,840 (Undeformed)

In the other experiment, stress-corrosion tests were conducted in duplicate at six different stress levels, varying from 45,000 to 70,000 psi in 5000-psi increments. The stress-corrosion tests were of the alternate-immersion type, and the test medium, 3-1/2 percent aqueous NaCl solution.

The starting material was the same for both experiments. It consisted of a 4- by 6- by 8-inch hand-forged -T73 billet conforming to Military Specification A-22771-B. The billet was cut into 1-1/4-inch-thick longitudinal sections, so -T73 heat treatments could be performed which would yield uniform properties.

RESULTS AND DISCUSSION

In agreement with the previous results, the stress-corrosion resistance of 7075-T73 was not found to be significantly affected by the prior deformation. As shown in Fig. 23, the t_f values varied between a low of 52 days, at a prestress level of 71,200 psi, and a high of 120 days, at a prestress of 70,000 psi. The two undeformed control specimens failed in 66 and 67 days, respectively.

The results from the present series of tests on highly stressed -T73 do not support the results obtained previously. It is seen in Fig. 2' that the time-to-failure tends to decrease, instead of increase, with increasing

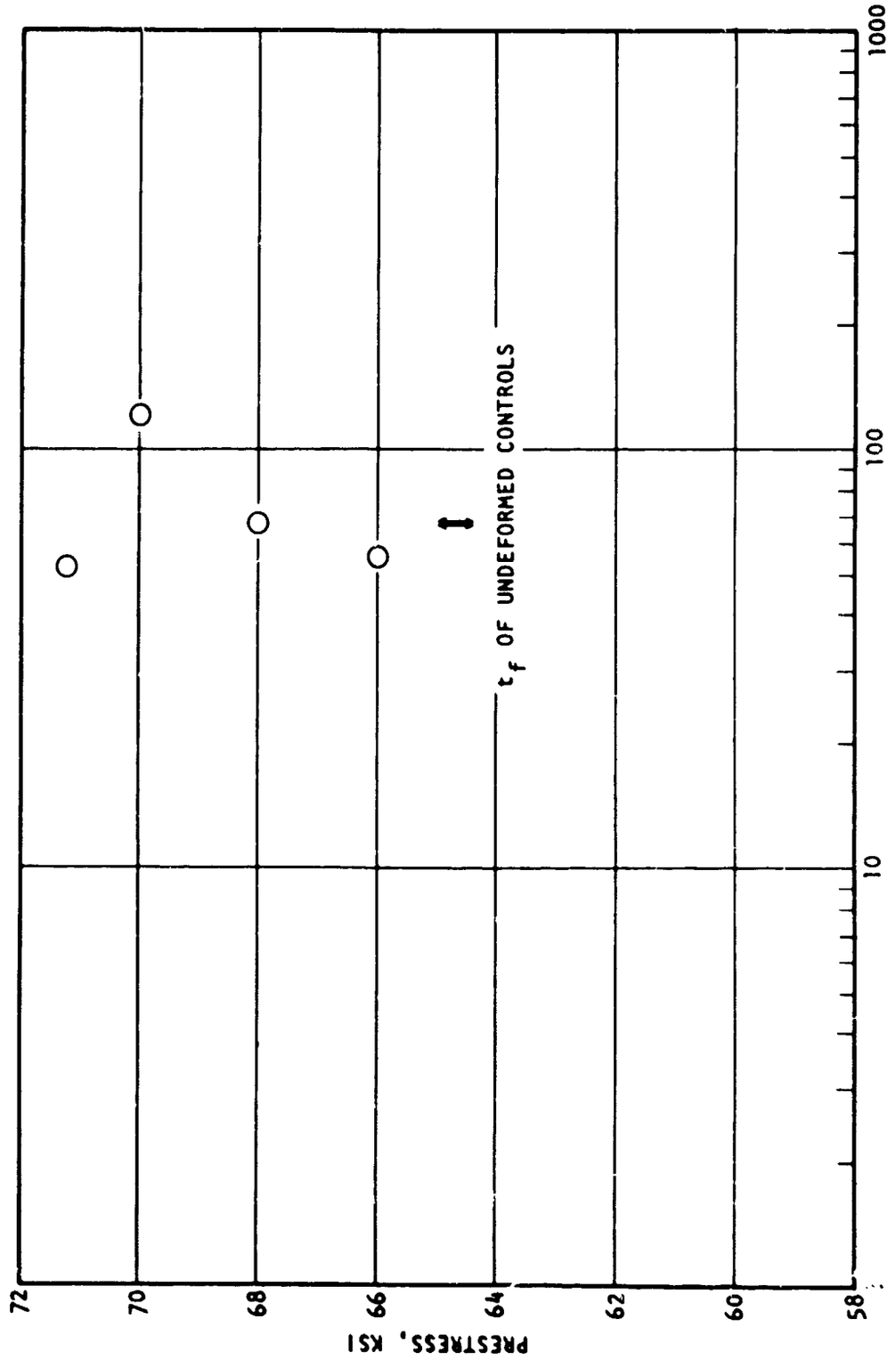

Figure 23. Deformation Prestress vs Time-to-Failure (t_f) of 7075-T73 Specimens

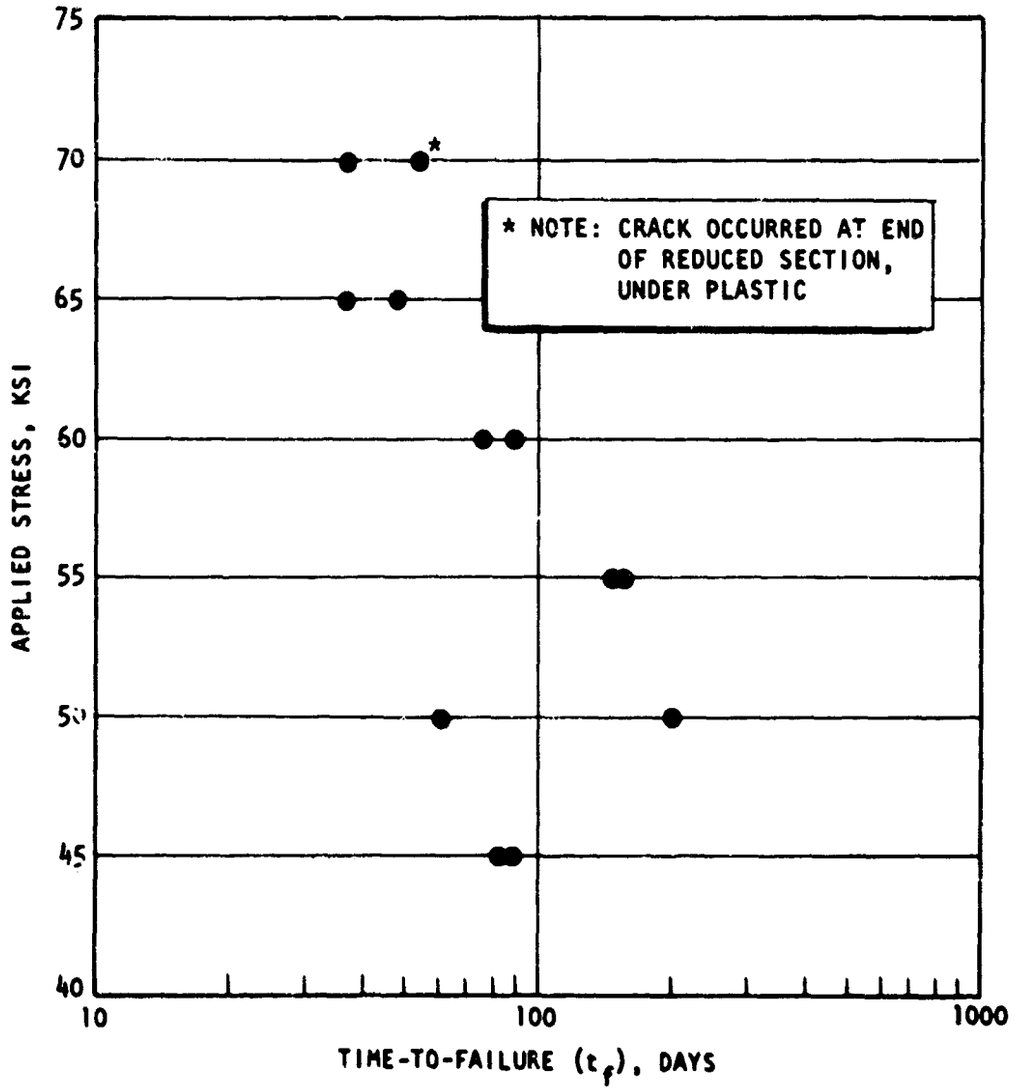

Figure 24. Applied Stress vs Time-to-Failure (t_f) of 7075-T73 Specimens

applied stress. The reason for the different results may be connected with the borderline stress-corrosion resistance of the material used previously. This borderline resistance was apparently unrelated to the tensile and conductivity properties which met specifications for -T73. However, it may have been related to a high degree of chemical and/or structural heterogeneity which could affect the environmental failure mechanism without, at the same time, influencing such macroscopic properties as yield strength. An additional series of tests on a "borderline" lot of -T73 should indicate whether the reproducibility of the previous results depends on the borderline stress-corrosion resistance itself.

DISCUSSION

The thin film study of plastically deformed 7075-T6 and -T73 and the measurements of dislocation mobility have confirmed that a significant difference exists between the two tempers regarding the ease of plastic deformation. The confinement of slip to a smaller number of planes in the -T6 suggests that fewer dislocation sources are operative than in -T73. However, slip is not only more difficult to initiate; it also propagates with greater difficulty because of more extensive strain aging. Any factor which activated additional slip systems or reduced the tendency toward strain aging would be expected to increase stress-corrosion resistance.

Important correlations have been found between stress-corrosion resistance, on the one hand, and particle size and macroscopic yield strength, on the other. The size of $MgZn_2$ particles apparently controls the ease of yielding but not the mechanism, according to the results of the cryogenic tensile tests on -T6 and -T73. The mechanism is similar in the two tempers and while showing a $T^{2/3}$ temperature dependence below 160 K, it is less dependent upon thermal activation above 160 K.

The small temperature dependence of the yielding mechanism in -T6 and -T73, at $T > 160$ K, is more indicative of a bypassing than of a shearing process. Thus, the slope changes observed in the particle-size, yield-strength, and time-to-failure curves at an over-aging time of 10 hours (350 F) would seem to suggest a transition from a higher to a lower degree of coherency between precipitate and matrix, rather than from a shearing to a bypassing mode of deformation. A classical dependence of yield strength on inter-particle separation and/or particle density was not borne out by the X-ray results. However, the $MgZn_2$ reflections were weak enough to cast reasonable doubt upon the volume fraction determinations which entered into the calculations of inter-particle separation and particle density. The thin-film examination of highly over-aged 7075 raised 7075 raised additional doubt concerning the X-ray intensity measurements.

The results of the amplitude-dependent internal friction measurements were very gratifying, considering the complex chemistry of the 7075 alloy. The usefulness of this technique as a tool for studying the aging kinetics in such an alloy has not been demonstrated before. The results not only support the Granato-Lücke model for dislocation damping, but more pertinent to the present discussion, they clearly show that during the early stages of aging when the predominant event is the formation of G.P. zones, one or more atomic species are diffusing to dislocations where they act as pinning points. The latter process must be entirely analogous to strain aging, which has been suggested as a critical factor in the stress-corrosion cracking mechanism.

CONCLUSIONS

1. Slip is more restricted in 7075-T6 than in -T73. Restricted slip is manifested by the arrangement of dislocations in discrete bands.

2. Following a rapid improvement in stress-corrosion resistance and a rapid decrease in yield strength during initial over-aging of 7075, a more gradual change in these properties was observed. These changes could be correlated best with the size of $MgZn_2$ particles as measured by X-ray techniques.

3. The temperature dependence of the yield strength of -T6 and -T73 is very similar over the temperature range from -423 F to ambient. The $T^{2/3}$ dependence exhibited at $T < 160$ K is suggestive of a shearing mechanism of plastic flow. A smaller temperature dependence was observed above 160 K.

4. Strain-rate sensitivity (SRS) measurements have demonstrated a higher strain-rate sensitivity ($1/m'$) in -T6 than in -T73. Strain aging occurs in both tempers but much more rapidly in the -T6. A tendency toward higher m' or m in the longitudinal as compared to the short transverse direction was also suggested by the SRS and stress relaxation measurements.

5. Amplitude-dependent internal friction measurements were successfully used to study early aging in 7075. The results were found to obey the Cottrell-Bilby model for strain aging and the Granato-Lücke model for dislocation breakaway.

6. The results of an earlier study on the effect of prior tensile deformation on the stress-corrosion susceptibility of 7075-T73 were checked and corroborated. The results of another study in which -T73 was stress-corrosion tested at stress levels above yield were not reproduced, perhaps because of the borderline stress-corrosion resistance of the starting material used previously.

FUTURE WORK

The objective of future work will be to apply the knowledge and improved understanding of the stress-corrosion mechanism in 7075 aluminum developed in previous programs to the optimization of properties of this alloy. Various over-aged conditons of the alloy possessing inherently high stress-corrosion resistance will be heavily deformed to increase the strength properties. The methods of deformation to be investigated will include conventional operations such as rolling and forging. Tensile and stress-corrosion tests will be conducted to determine the thermal-mechanical treatment producing the best combination of yield strength and stress-corrosion resistance.

REFERENCES

1. Jacobs, A. J., "Study of Stress-Corrosion Cracking of Aluminum Alloys," Naval Air Systems Command, Contract NOw 66-0309d, Final Report, 6 April 1966 to 5 April 1967 (May 1967).
2. Jacobs, A. J., "The Role of Dislocations in the Stress-Corrosion Cracking of 7075 Aluminum Alloy," A.S.M. Trans., 58, 579 (1965).
3. Holl, H. A., Corrosion, 25, 173 (June 1967).
4. Speidel, M. O., "Interaction of Dislocations With Precipitates in High Strength Aluminum Alloys and Susceptibility to Stress Corrosion Cracking," paper presented at the International Conference on Fundamental Aspects of Stress-Corrosion Cracking, Columbus, Ohio, 11-15 September 1967.
5. Ryum, N., et al., "Brittleness and Microstructure of Some Al-Mg-Zn Alloys," Z. Metallkde, 58, 28 (1967).
6. Thomas, G. and J. Nutting, J. Inst. Met., 88, 81 (1959/60).
7. Swann, P. R., Corrosion, 19, 102 (1963).
8. Hsiao, C. C., Physics Today, 19, 49 (1966).
9. Zhurkov, S. N., Int. J. Fracture Mech. 1, 311 (1965).
10. Laves, F. and J. Löhberg, Nach. Acad. Wiss. (Göttingen) 1, 59 (1934).
11. Stokes, A. R., Proc. Phys. Soc., London, 61, 382 (1948).
12. Warren, B. E., Prog. in Met. Phys., 8, 147 (1959).
13. Hickman, B. S., J. Aust. Ceramic Soc., 3, 21 (1967).
14. Gensamer, M., "Strength of Metals Under Combined Stresses," p. 22, American Society for Metals, Cleveland, Ohio (1941).
15. Kelly, A. and R. B. Nicholson, "Precipitation Hardening," Progress in Materials Science, Vol. 10, No. 3, The MacMillan Co., New York (1963).
16. Orowan, E., "Dislocations in Metals," p. 131, A.S.M. (1954).
17. Byrne, J. G., M. E. Fine, and A. Kelly, Phil. Mag., 6, 1119 (1961).

18. Matsuura, K. and S. Koda, Phil. Mag., 6, 1531 (1961).

19. Guard, R. W., Acta Met., 9, 163 (1961).

20. Johnston, W. G. and D. F. Stein, Acta Met., 11, 317 (1963).

21. Schadler, H. W., Acta Met., 12, 861 (1964).

22. Hull, D. and F. Noble, Disc. Far. Soc., 38, 251 (1964).

23. Johnston, W. G., J. Appl. Phys., 33, 2716 (1962).

24. Chang, R., "The High Temperature Mechanical Properties of Solids From Stress Relaxation Experiments," paper to appear in Proceedings of the Third International Symposium on High Temperature Technology, Stanford Research Institute (1967).

25. Jacobs, A. J., "The Mechanism of Stress-Corrosion Cracking in 7075 Aluminum," paper presented at the International Conference on Fundamental Aspects of Stress-Corrosion Cracking, Columbus, Ohio, 11-15 September 1967.

26. Brummer, S. B., et al., "Study of the General Mechanism of Stress Corrosion of Aluminum Alloys and Development of Techniques for Its Detection," NASA Contract No. NAS8-20297, Fourth Quarterly Report, 1 June to 31 August 1967.

27. Chang, R., "A Stress Relaxation Approach to Probing the Deformation Behavior of Crystalline Solids," Unpublished Technical Report, North American Rockwell Corporation (1967).

28. Holt, D. L., et al., "The Strain-Rate Dependence of the Flow Stress in Some Aluminum Alloys," A.S.M. Trans., 60, 152 (1967).

29. Thompson, D. O. and F. M. Glass, Rev. Sci. Inst., 29, 11, 1034 (1958).

30. Cottrell, A. H. and B. A. Bilby, Proc. Phys. Soc. A 62, 49 (1949).

31. Granato, A. and Lücke, J. Appl. Phys., 27, 6, 583 (1956).

32. Metals Handbook, Eighth Edition, Vol. 1, p. 948 (1961).

33. Jacobs, A. J., "The Effects of Point Defects and Dislocations on the Stress-Corrosion Susceptibility of Aluminum Alloys," NASA Contract No. NAS8-20471, Final Report, 25 February 1968.

Unclassified

Security Classification

DOCUMENT CONTROL DATA - R & D

(Security classification of title, body of abstract and indexing annotation must be entered when the overall report is classified)

1. ORIGINATING ACTIVITY *(Corporate author)*
Rocketdyne, a Division of North American Rockwell Corporation, 6633 Canoga Avenue, Canoga Park, California 91304

2a. REPORT SECURITY CLASSIFICATION
Unclassified

2b. GROUP

3. REPORT TITLE
The Role of Dislocations in the Stress-Corrosion Cracking of Aluminum Alloys

4. DESCRIPTIVE NOTES *(Type of report and inclusive dates)*
Final Report, 6 May 1967 through 5 May 1968

5. AUTHOR(S) *(First name, middle initial, last name)*
A. J. Jacobs

6. REPORT DATE	7a. TOTAL NO. OF PAGES	7b. NO. OF REFS
June 1968	76 & vii	33

8a. CONTRACT OR GRANT NO.	9a. ORIGINATOR'S REPORT NUMBER(S)
N00019-67-C-0466	R-7476
b. PROJECT NO.	
c.	9b. OTHER REPORT NO(S) *(Any other numbers that may be assigned this report)*
d.	

10. DISTRIBUTION STATEMENT

11. SUPPLEMENTARY NOTES	12. SPONSORING MILITARY ACTIVITY
	NASC, Washington, D. C.

13. ABSTRACT

A thin-film examination of plastically deformed 7075-T6 and -T73 has shown that slip is confined to a smaller number of planes in the -T6 than in the -T73. X-ray line broadening measurements of ($MgZn_2$) particle size in a series of overaged 7075 conditions, together with stress-corrosion and tensile tests, have indicated that a correlation exists between particle size, time-to-failure, and yield strength. Each of these quantities undergoes a rapid change during the first 10 hours of aging at 350 F, and a much slower change thereafter. In cryogenic tensile tests, the yield strengths of -T6 and -T73 were shown to have a similar temperature dependence: the $T^{2/3}$ dependence, which is suggestive of a shearing mechanism, was obeyed from 20 to 160 K, and a smaller dependence was exhibited from 160 to 300 K. Dislocation mobility measurements have demonstrated a higher strain-rate sensitivity in -T6 than in -T73, and also a stronger tendency toward strain aging in the former temper. Amplitude-dependent internal friction studies have provided insight into dislocation-precipitate interactions, as well as into the early aging process in 7075.

DD FORM 1 NOV 65 1473

Unclassified

Security Classification

14 KEY WORDS	LINK A		LINK B		LINK C	
	ROLE	WT	ROLE	WT	ROLE	WT
Stress Corrosion						
7075 Aluminum						
Plastic Deformation						
Thin Films						
X-rays						
Tensile Tests						
Dislocation Mobility						
Internal Friction						